Energy Reports 9 (2023) 3967–3988

Contents lists available at ScienceDirect

Energy Reports

journal homepage: www.elsevier.com/locate/egyr

Research paper

Participation of load aggregator in grid frequency stabilization with consideration of renewable energy resources integration

Emmanuel Mudaheranwa [a,b,*], Hassan Berkem Sonder [a], Ye-Obong Udoakah [a], Liana Cipcigan [a], Carlos E. Ugalde-Loo [a]

[a] School of Engineering, Cardiff University, Cardiff, UK
[b] Department of Electrical and Electronics, IPRC Karongi, Rwanda polytechnic, Rwanda

ARTICLE INFO

Article history:
Received 30 October 2022
Received in revised form 16 February 2023
Accepted 6 March 2023
Available online xxxx

Keywords:
Distributed generation
Aggregator
Demand response
Frequency control
Renewable energy
Sustainability

ABSTRACT

Alterations in the proportion of conventional generation to that of renewable energy source could be a future challenge for electric energy networks. Conventional power plants are being replaced by wind and solar energy. Solar PV plants and wind turbines lower the system inertia constant, causing the grid frequency to shift. Renewable energy generation plants that are integrated into the energy system may cause problems with frequency stability if adequate frequency control techniques are not applied. In this study, a Load Frequency Control framework based on aggregators is developed to improve the frequency response of the power system. It was demonstrated that the aggregator is capable of forecasting available flexibility for the day ahead contributing to the frequency control process. The aggregator is contributing to the grid frequency stabilization considering the price signal for minimizing energy costs, with an effect on end user's energy bills reduction. For assessing the aggregator's flexibility availability, the aggregator calculates the contributed power after minimizing its energy costs. The results show that it is possible to use DR technology to stabilize the grid frequency. With the loss of generation of 50 MW, the aggregators contribute mainly for the morning event with a contribution of about 4 MW followed by the night event with the contribution of approximately 3.5 MW. The largest contribution was obtained between 06:00 and 8:00 for the examined area with three aggregators, and the smallest contribution was obtained between 22:00 and 24:00. By considering the whole power system, with the integrated renewable energy resources in different periods, the findings demonstrate that even though the frequency decreases, it quickly returns to the usual operating limit and stabilizes itself back to the normal operating limits of 50 Hz as a result of the aggregator participation in the process of grid frequency stabilization.

1. Introduction

As a result of the fact that customers may go through times of insufficient or excessive electricity supply, it is viable for aggregators to offer customers services that either raise or reduce the amounts of electricity that they use. If there is a surplus of power or insufficient of it, an aggregator is capable of lowering the demand (also known as providing flexibility) in accordance with this information. In generally, generating and reserve units are required to make adjustments to the generated power in response to the variations in demand in order to maintain an operating frequency that falls within the normal pre-set limits (which is 50 Hz for the considered case study). Because it was shown that the future system's inertia would be lower as a result of changes in the use of alternative electricity generation from solar or wind, the existing strategies of controlling the frequency will not be enough (Dehghanpour and Afsharnia, 2015). As a consequence of renewable energy sources integration, additional frequency control provision is necessitated to guarantee that the renewable energy sources dependable services are provided without the violation of power grids security, reliability, stability, and its dynamic steady state operations.

Regarding the situation in Rwanda, the research referred to in Mudaheranwa et al. (2022) showed that the existing conventional power sources would not be capable of absorbing the variability in power generations output from renewable power (i.e, PV) and imported electricity penetration. This conclusion was reached after conducting an analysis of three different possible futures for the modern technology of renewable energy generation. As a result of the aforementioned, the frequency may end up deviating above or below the safe operating limits as a consequence. During

* Corresponding author at: School of Engineering, Cardiff University, Cardiff, UK.
E-mail addresses: mudaheranwae@cardiff.ac.uk, mudanwa@yahoo.com (E. Mudaheranwa).

https://doi.org/10.1016/j.egyr.2023.03.034

Abbreviations

AGC	Automatic Generation Control
ANSI	American National Standards Institute
DER	Distributed Energy Resources
DG	Distributed Generator
DSO	Distribution System Operators
EV	Electric Vehicle
ICA	Imperialist Competitive Algorithm
LA	Load Aggregator
LCE	Loading Control Error
LFC	Load Frequency Control
LRC	Loading regulation capacity
MFLN	Modified Functional-Link net
PHSS	Pumped Hydroelectric Storage System
REG	Rwanda Energy Group
RES	Renewable Energy Resources
SDGs	Sustainable Development Goals
TSO	Transmission system operator
SOS	Symbiotic Organism Search
PSO	Particle Swarm Optimization

Symbols and Units

P_{ni}^{0}	The detected available power (forecasted flexibility) in MW.
P_{ni}^{max}	The Aggregator maximum power (MW).
P_{gi}^{max}	The AGC maximum power (MW).
N	Number of aggregators.
P_{ni}^{a}	Aggregator allowable minimum contribution power (MW).
i	Subscript referring to area $i = 1,2\&3$
H_{i}	Inertia constant of area i
R_{i}	Aggregate speed regulation of area i
D_{i}	Load frequency characteristics of area i
"z_{i}	System stiffness
T_{ghi}	Governor time constant of the hydro power plant in control area i
T_{gti}	Governor time constant of the thermal power plant in control area i
T_{ij}	Synchronizing power coefficient (pu) between area i and j
T_{tti}	Thermal turbine time constant of area i
T_{thi}	Hydro turbine time constant of area i

the high progression scenario, the calculated value of the inertia constant could drop from 7.2 s to somewhere around 3.83 s, which would result in drop in frequency of around 46.45 hertz (roughly 7.5 percent just under the standard frequency of operation, which is set at 50 Hz). According to the estimates, by the year 2050, the grid will have seen more significant variations and oscillations as a result of a higher renewable energy source integration into the grid. As a result, there is a possibility that the system will become unstable.

Following power disruptions, the analysed frequency response demonstrated that the frequency somehow does not stay within the established limits. As a contribution in this regard, this study presents a new approach for controlling the frequency by taking into consideration the involvement of demand-side management.

Classical approaches for automatic generation control (AGC) are typically suitable for particular frequency operation conditions. On the other hand, taking into consideration the proliferation of new microgrids and renewable energy sources, this AGC strategy may no longer be appropriate for the future's power systems.

Some research publications have provided more advanced solutions that assist frequency control by focusing on demand response and adaptability. The purpose of the article (Villena et al., 2015) is to analyse the demand-side contributions to frequency management. In it, the authors examine and outline a comprehensive process for determining essential wind fluctuations in power grids that have a large presence of wind. The research presented in Zhu et al. (2017a) addresses the modelling and control method for LFC and DR in a deregulated power system. This research takes into account the many temporal delays that are caused by the use of channels of communication. In addition, a description of the general idea behind DR programs as well as its classification can be found in Wu and Tang (2019). This is then accompanied by a focus on the particular concept of Direct Load Control (DLC) and Extended Demand Response (EDR) programs. Latif et al. (2020) investigates the role that price-based demand response (PBDR) plays in frequency control by employing a hybrid microgrid system to conduct their research. This particular microgrid plan incorporates diesel engine generators, wind turbine generating systems, solar thermal power systems, fuel cells, and aqua electrolyzers into its infrastructure.

A survey of the relevant literature indicates that a number of LFC strategies have been suggested for use in interconnected power networks. These methodologies have made substantial contributions to the early development of LFC operation (Zhu et al., 2017b; Silva and Assis, 2020). However, at the same time, it has been noted in this research report that the majority of the investigators have worked on load frequency management difficulties that are confined to the conventional interconnected power system. The conventional resources are decreasing on a daily basis, and at the same time, the demand for power is also growing; hence, there is a greater focus placed on the inclusion of renewable energy sources (RES) (Kerdphol et al., 2019; Ahmed et al., 2021). The magnificent benefit of the suggested use of RES is that it does not produce any carbon emissions, it is a clean source, it is readily available, and it is both good to the environment and the economy (Saxena et al., 2020; Marzebali et al., 2020). Interconnected power networks are impacted in two different ways when conventional energy sources like solar photovoltaic and wind turbines are occasionally replaced by intermittent non-conventional energy sources. Both a decrease in the system's inertia and intermittent generation are major contributors to frequency stability getting worse with time (Datta et al., 2019; Agostini et al., 2021). As a result, a high penetration rate can indicate that there are specific problems with voltage instability, frequency deviation, poor power quality, or reliability obstruction. For the purpose of mitigating the aforementioned issues and increasing the proportion of renewable energy sources (RES) in the electric power system (Joung et al., 2019; Das et al., 2020), a fresh point of view and an original ideology are required.

Studies have proposed that energy storage (ES) systems are a viable option that has the ability to overcome the unfavourable impacts that are caused by the lowering of inertia caused by RES (Xu et al., 2018; Arya, 2020). The energy storage component is responsible for supplying the injected power in the event of unexpected fluctuations in demand, which helps to maintain the consistent frequency of the load. It is possible for the microgrid's reserve power in energy storage (ES) elements to raise the inertia property, which will result in a more stable load frequency (Debbarma and Dutta, 2017; Vinoth Kumar and Thameem Ansari,

2016). Therefore, a high-power density storage system such as super capacitor energy storage (SCES) (Saha and Saikia, 2018; Kumar et al., 2018), superconducting-magnetic-energy-storage (SMES) (Salama et al., 2019; Wang et al., 2018), and flywheel-energy-storage (FES) (Hassanzadeh et al., 2020) can be merged with BES in order to regulate greater surge currents in a cost-effective manner. These are currently under consideration for the purpose of storing unused energy and supplying that energy during times of high load demand. The literature review makes it abundantly clear that LFC has an enviable position in future power scenarios that investigate some renewable energy sources that have not yet been fully investigated (Xi et al., 2020a).

It has been observed, in light of what has been said above as well as the examination of previous research works, that researchers are constrained to and predisposed toward the standard LFC formulation. However, because of shifts in lifestyle, the ongoing depletion of conventional sources of energy, and increases in supply and demand, renewable energy sources and the application of those sources are playing an essential role in addressing the issues that have been raised. Because of this, the purpose behind the present work, which deals with the incorporation of RES into both the traditional and modern LFC approach, is reinforced.

Although the references discussed in the literature review consider Demand Response (DR), but the significance of flexibility is often disregarded. To bridge this research gap, a framework for the provision of frequency response services facilitated by an aggregator is presented in this study.

Demand for electricity should be regulated, and the aggregator plays an important role in this. The control of demand by the aggregator is done by either raising the amount of energy supplied when there is a rise in the quantity of energy requirement or by raising the energy consumed when there is a rise in the quantity of power delivery. The measurement of system frequency, followed by the implementation of load limitation or load shedding mechanisms in reaction to that detection, is what causes changes to the consumption levels (known as incentive based direct load control). It is essential to have a load aggregator in order to exercise control over the overall amount of load that is necessary in order to keep a record of the intended amount of power consumption. It acts as a bridge connecting customers and the administrator of the grid, making decisions that take into account the advantages enjoyed by customers as well as those of the overall system.

By considering the operation of a wide range of renewable energy sources and load management system, the study investigates the reduction of the total reliance on electricity from the grid, in day-ahead and real-time energy markets, while also balancing an anticipated load.

1.1. Load aggregators and their impact on energy systems

The aggregator has the ability to limit usage (flexibility provision) depending on whether electricity is in abundant supply or even in limited supply as shown in Fig. 1.

In the past of vertically integrated power utilities, the same corporation was often responsible for the generation of electricity, operation of the network, and supply of final customers. This model has since become less common Distribution System Operators (DSOs), in power networks that have been liberalized, may be required to accommodate a range of energy suppliers inside their grid domain. On the other hand, suppliers might participate in multiple grid systems at the same time (Hadi, 1999; Prabha et al., 1994).

The electricity market facilitates the exchange of energy between suppliers and producers. In addition, companies that produce electricity are expected to compete for control reserves

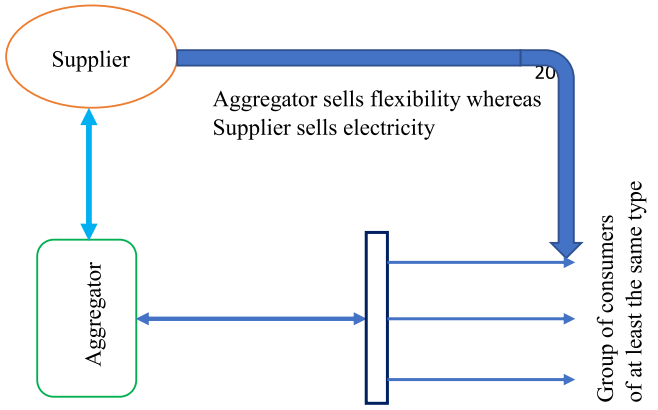

Fig. 1. Block diagram of aggregator as flexibility provider.

and other grid services which are managed by Transmission System Operators (TSOs). These services are referred to as "ancillary service markets". In order to ensure that conditions are not discriminatory, it is a standard practice for grid operators to place limits on the information that can be shared with market participants (Koch, 2015). This has a number of repercussions, particularly for the implementation of "Smart Grid" capabilities within electricity distribution networks. In the context of smart grids, new capacities and technologies are put in place to promote increased information flow and correspondence amongst all parties concerned. This helps make the system more efficient. These include generation companies, system operators, market players, and distribution system load aggregators (Anon, 2011). In this section, load aggregators and the influence they have on the global landscape of electrical systems are discussed.

1.2. Load aggregator concepts

A Load-Serving Entity, often known as an LSE, is an entity that connects the consumers and the market for electricity (Anon, 2022a). In its early days, LSE is primarily involved in the business of buying and selling power. It is also the company that came before Load Aggregators (LAs). As a result of the increased utilization of demand-side resources, LA evolved from a section of LSE into a more specialized entity responsible for the integration of DR resources (Saad et al., 2009).

In order to engage in the power system market or offer services to system operators as a single entity, different agents in the power system, such as consumers and producers or consumers with other combinations, are characterized by Burger et al. (2017) as aggregation. To summarize, LA is a coordinator of DR's available resources. LA operates as a communication entity between grid businesses and power users, making efficient use of idle and distributed load resources. Additionally, Load aggregators perform the function of a gateway connecting energy consumers and service providers by integrating and regulating load resources on the consumer side (i.e., virtual power plants). Aggregators are relatively recent additions to the world of electricity systems. They are equipped with the capacity to exert their influence over a number of grid-connected units by means of an appropriate communication interface. In order for the units to cooperate and achieve a predetermined control objective as a whole, coordination is typically accomplished through centralized optimization. The units in an aggregator's portfolio can be used for trading in the electricity and ancillary service markets.

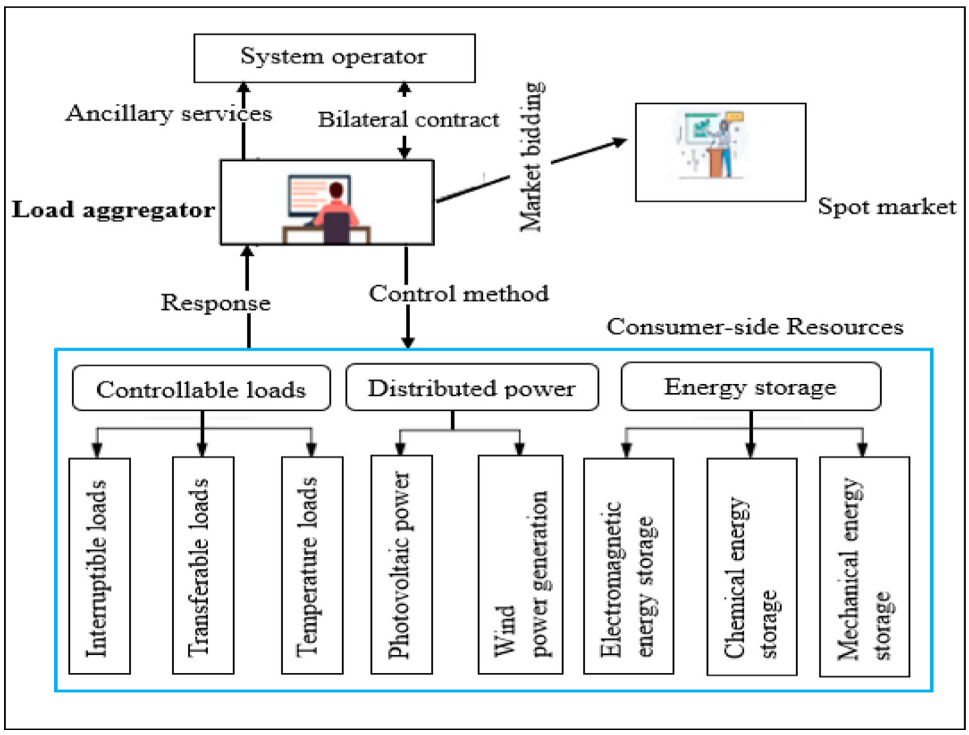

Fig. 2. Operation structure of load aggregator in electric power system.

Controllable loads, distributed power sources, and energy storage devices are the three sorts of resource types that fall under the purview of the LA control system.

Controllable load. There are three distinct classifications that are used to categorize loads that have the possibility to be deployed. These categories are transferable loads, reducible loads, and thermostatically regulated loads. Anon (2022b) and Udoakah et al. (2019) state that the definition of transferable load is the load that has a fixed level of power usage during the entire scheduled period with a beginning that is reasonably changeable. A load is referred to as "reducible load" when it possesses a particular level of adaptability and operability in terms of its operating time and the quantity of electricity it requires. This load is characterized by its ability to modify its status in order to meet the demand that is being imposed on the network, as well as by its flexible scheduling, rapid reaction, and limited capacity for aggregation. Air conditioning, water heaters, and other loading are frequently included in the category of thermostatically regulated loads. Thermostatically controlled loads are distinguishable from other types of loads due to their rapid reaction, their capability to store energy, and their greater standard of manoeuvrability.

An autonomous energy supply system that is deployed at the consumer end, is what **distributed generation** is described as Xu et al. (2011a). The broad adoption of green sources on the consumer end tends to increase the planning control range of the system, that also allows the consumer side to use the electric power all the while operating as the supply to send power to the grid. This is made possible by the fact that the user side makes extensive use of renewable energy. They exist many different kinds of distributed generators, and each of these sources has its own set of distinctive characteristics. For example, photovoltaic renewable power can only be produced during daytime, while wind power seems to have the capacity to control peak load.

Fig. 2 provides a visual representation of the organizational make-up of LA's workings.

1.3. Load aggregator responsibility on the side of user and the power market

On the user side, the LA operation mostly consists of installing intelligent monitoring and providing technical assistance, carrying out an analysis of the user's DR capacity, designing an incentive mechanism, and scheduling and planning in ahead. It is necessary for LA to investigate the many kinds of loads and the DR potential of each, as well as to comprehend the degree to which the loads of the various electricity-using equipment vary.

Individualized agreements are negotiated with customers on the basis of their individual patterns of power usage (past data, such like response time and curtailment), the limits imposed by their usage habits, and their commitment to reduce their power consumption. The purpose of these contractual agreements is to establish the much more appropriate customer service available in order to schedule their involvement in a specific market in order to maximize the use of resources, as well as to maximize the influence and importance of DR commitment in the market (Anon, 2009; Ming et al., 2020). This is done in order to maximize the potential for profit from DR's willingness to participate in the business.

As far as the incentives are concerned, a suitable incentive structure is an absolute necessity if one wishes to successfully persuade customers to take an active role in the programs that are offered by LA. The rates of compensation are decided by LA after consulting with the user and are based on the particular kind of service that is being given. These rates are provided by LA. It is required to build a penalty mechanism to limit user behaviour in order to prevent the unstable operation of the system that is produced by an excessive number of consumers not responding to the system's requests. In addition, LA is required to give careful regard to the satisfaction, level of comfort, and power usage trends of the consumers (Angel and Mansueti, 2009).

The LA needs to prepare ahead for its scheduling demands and keep customers informed. In order to arrive at the most cost-effective combination of scheduling options, the formulation of

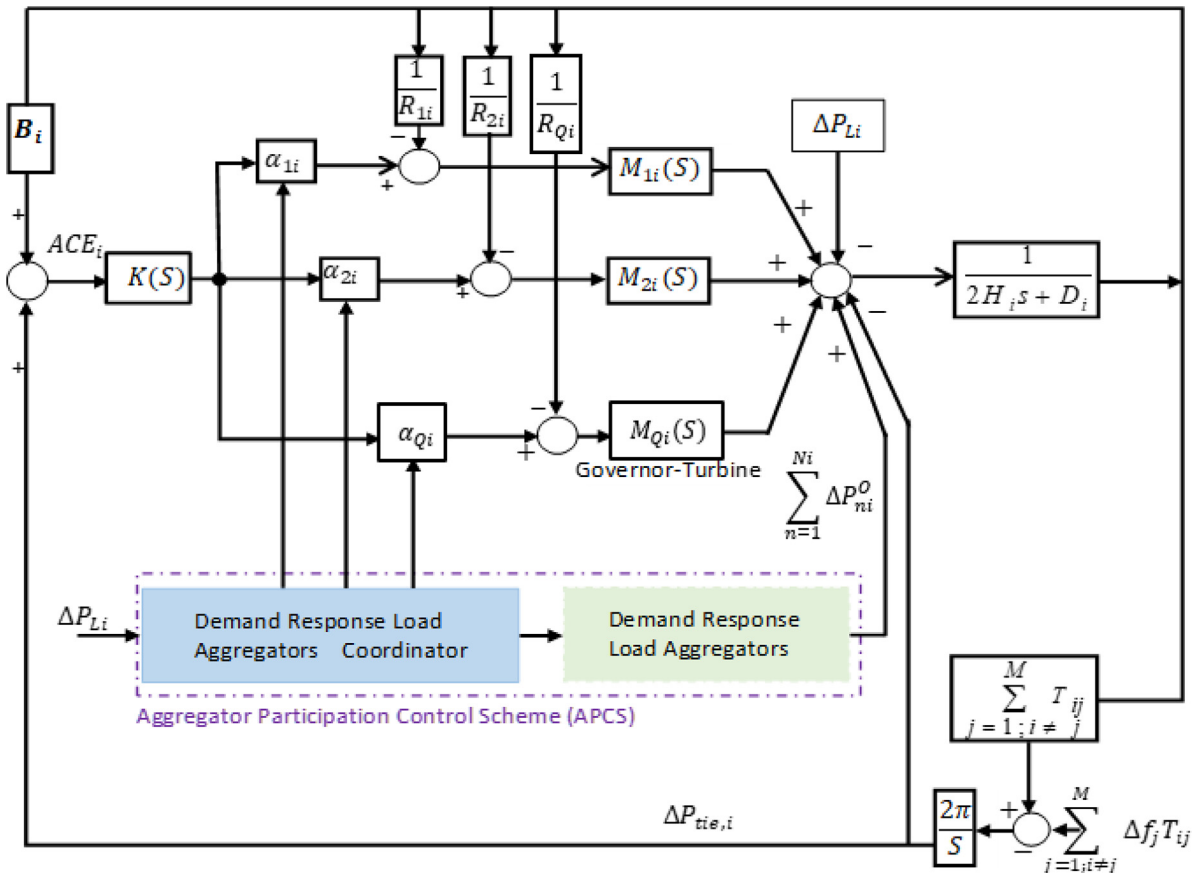

Fig. 3. Frequency control block diagram with the participation of LA.

the scheduling plan needs to take into account reducing costs in its full extent, the possibility of consumer insolvency, and the requirement to meet the constraints of consumer intrusion time, lower and higher cutting timing (Gholian, 2016; Parvania, 2014; Ruiz, 2009).

2. Research elaboration

2.1. Proposed aggregator's coordination model

As a result of the imbalance between load and generation, the frequency of a power system oscillates around the traditional system frequency (e.g., 50 Hz). Consequently, robust measures need to be implemented to return frequency to its nominal operational value. It is assumed that each control area should have one or multiple LAs, each of which must have maximum regulation capacity ($P_{ni.}^{max}$).

Additionally, the LA in each control area is overseen by a coordinator. The power mismatch (ΔP_L) between each region is estimated from the area control error (ACE) signal in the transient phase when there is an imbalance in power. Based on the ACE, an investigation into the power provision technique for AGC units during the period in which LAs are introduced within each control region is carried out. Through consideration of the regulation capacity limits $\left[P_g^{\min}, P_g^{\max}\right]$ of AGC units and LAs, the goal is to determine how this imbalanced power is shared between them. During implementation of the presented control scheme, a LA coordinator is proposed, which generates an electronic coordination signal that is transmitted to all LAs. The LFC method with the participation of LA of *ith* control area is shown in Fig. 3.

Given that N represents the number of LAs and Q represents the number of generating units in the *ith* control area. Based on the theory presented in Anon (2021a), the frequency control model is given as in (1).

$$\Delta f_i(S) = \frac{1}{2H_i + D_i}\left\{\left(\sum_{n=1}^{Ni}\Delta P_{ni}^{O}(S) - \Delta P_{Li}(s) + \sum_{q=1}^{Qi} M_{qi}(S)\left[\Delta Pc_{qi}(s) - \frac{1}{R_{qi}}\Delta f_i(S)\right]\right) - \Delta P_{tie,i}\right\} \tag{1}$$

Where M_{qi} is calculated as in (2):

$$M_{qi} = \frac{1}{(1 + T_{gqi}S)} \cdot \frac{1}{(1 + T_{tqi}S)} \tag{2}$$

With: T_g representing the governor time constant. T_t denoting the turbine time constant. The tie-line power deviation is defined as in (3):

$$\Delta P_{tie,i(S)} = \frac{2\pi}{s}\left[\sum_{j=1,j\neq i}^{M} T_{ij}\left(\Delta f_i - \Delta f_j\right)\right] \tag{3}$$

The overall power imbalance is adjusted by both the available capacity (ΔPc) to be provided by generating units and the LAs (ΔP_{ni}^{O}) in steady state.

As a result, the new equilibrium equation for control area i is given by (4):

$$\Delta P_{Li} = \sum_{q=1}^{ni}\Delta P_{Cqi} + \sum_{n=1}^{Ni}\Delta P_{ni}^{O} \tag{4}$$

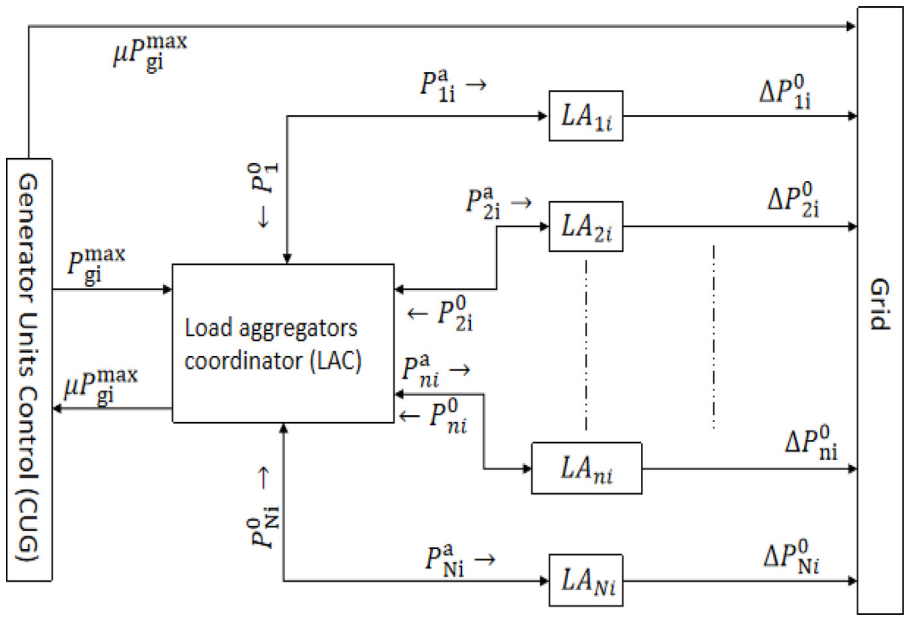

Fig. 4. Schematic diagram representing the control layout of the LA.

To ensure that all LAs have an equal opportunity to participate in the grid frequency stabilization, the required active power is allocated in the same proportion as the maximum possible active power control capability for every LA (P_{ni}^{max}). For example, assuming that $P_{ni}^{O}(t)$ is the active power of the *nth* LA under present conditions, a fair regulatory issue among numerous LAs requires that each one should operate at the same ratio (γ), which is referred to as coordinated consensus participation, described by (5):

$$\frac{P_{1i}^{O}}{P_{1i}^{max}} = \frac{P_{2i}^{O}}{P_{2i}^{max}} = \cdots = \frac{P_{Ni}^{O}}{P_{Ni}^{max}} = \gamma \tag{5}$$

As both AGC and LAs share the imbalanced power in the control area, which is divided among them, the dividing ratios (μ) of AGC capability, and that of LAs (γ) are introduced. The coordinator initiates the participation of the LAs by transmitting a control signal (γ) to the participants.

Fig. 4 depicts the control of the LA's participation. The electric power provided by each LA is calculated with the assistance of the logic depicted in the schematic diagram, which is consistent with the control algorithm outlined in (5).

The ACE is detected by the LAC, which then queries each LA for their contribution to the minimum and maximum available power. To ensure that each LA has an equal opportunity to participate in the market, the LAC calculates the amount of electricity to be given using (5) and communicates the result to each aggregator and generator. After comparing the available maximum and minimum power at each LA, the control signal (γ) is obtained as shown in Fig. 5, where the contributed power by the aggregators is computed as well. In Fig. 5, the following nomenclature is adopted:

P_{ni}^{0} is the detected available power (forecasted flexibility).
P_{ni}^{max} is the Aggregator maximum power.
P_{gi}^{max} is the AGC maximum power.
N is the number of aggregators.
P_{ni}^{a} is the Aggregator allowable minimum contribution power.

2.2. Analysis and estimation of the aggregator's potential contribution

It is possible for a grid trader to participate in the wholesale market without or with an agreement with an aggregator. There is also the possibility of entering into contractual agreements with aggregators in order to take care of its locally connected load. Aggregators are allowed to enter into bilateral agreements with network operators and consumers in order to offer load-side control services and energy subsidies. In addition, the aggregator has the ability to act as a reseller for the grids, and as a result, it has the ability to grant the accessibility to the wholesale market. Both the wholesale market and the Distribution System Operator (DSOs) will be able to take advantage of the aggregator's services. Customers' resources related to the units of the relevant DSO are used to improve services delivered to that the DSO.

The aggregator's contributing power is estimated by evaluating the flexibility of customers' grid integration under the constraints of a given pricing incentive signal provided by the aggregator. EMS optimization from the aggregator's point of view, price inducement signal deployment, and the ultimate generation of changes in loading condition are the purposes of this study.

The method of scheduling and operating methods that is described in Coppl et al. (2020) and Xu et al. (2011b) is utilized in this study. Within this method, there are clusters, and the average consumer is used to represent each cluster. Following the completion of a separate simulation of the EMS for every customer, the results are then summed by multiplying with the overall number of prosumers.

In addition, the GAMS (Bussieck and Meeraus, 2002) and MATLAB software were used in the creation of the flexibility forecasting tool.

2.3. The determination of the power contribution made by the aggregator

The demand and generation units are the elements that are engaged in the load management flexibility for customers. This flexibility is provided by the demand response. The following is a detailed breakdown of the categories that they fall into:

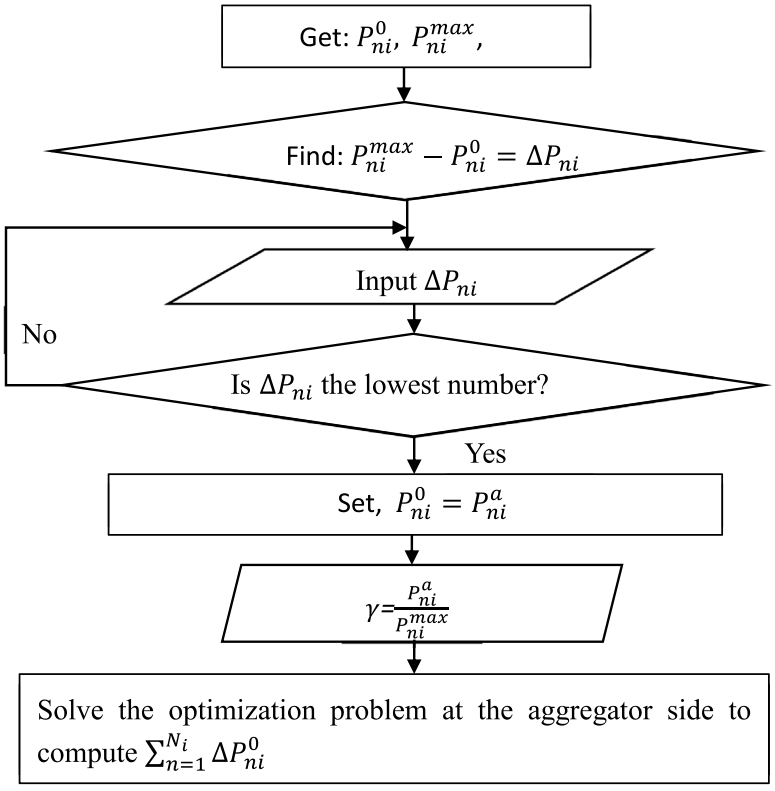

Fig. 5. Proposed algorithm to coordinate the aggregators.

Critical load: refers to the appliances which demand has to be satisfied at all times and is unmanageable. This consumption must always be met no matter what.

Shiftable load: Since these appliances must run continually for a certain amount of time once they have been switched on, their usage can be postponed until a later point in time.

Electric Vehicles (EVs): Electric vehicles are an essential component of system flexibility due to the fact that it is anticipated that they would function in both directions. The modelling technique takes into account a number of crucial factors, including the electric vehicle batteries' maximum and minimum states of charge (SoC), as well as the driving patterns that are analysed for each of the batteries.

Renewable Energy Resources: Solar PV plants are being investigated as a potential source of renewable energy.

Assuming that *Cc* is the cost of grid connectivity, *Hp* is the predicted price one day ahead in the spot market, EV_C^{disch} is the cost of EV battery degradation, and π^{puns} is the price of "unsupplied demand penalties. This will create a mathematical model for the optimal power contribution. The goal is to bring down the energy expenses of the aggregator as much as possible, which will in turn bring down the energy bills of the final user. By solving the following optimization problem, one can determine the cost that is the lowest possible:

$$\min \sum_{t=1}^{T} \left[H_a \left(P_t^{buy} + P_t^{sell} \right) + C_a \left(P_t^{buy} - P_t^{sell} \right) \right] + \sum_{t=1}^{T} \sum_{v}^{V} \Delta_T \left[EV_C^{disch} P_{t,v}^{EVdisch} \right] + \sum_{t=1}^{T} \pi^{puns} d_t^{unsup} - \sum_{n}^{N} \sum_{t_i}^{t_f} \left(1 - x_{n,t} \right) I_{n,t} \quad (6)$$

in which P_t^{buy} is the amount of power that was bought from the grid, P_t^{sell} is the amount of power that was sold to the grid, $P_{t,v}^{EVdisch}$ is the rate at which electric vehicles are discharged, d_t^{unsup} is the amount of unmet critical demand, and $x_{n,t}$ and $I_{n,t}$ are the incentive activation and the incentive that is given to consumers, respectively. The times t_I and t_f, respectively, denote the beginning and closing times of the incentive.

The corresponding constraints on the previous components will need to be relaxed a bit in order to solve the dual problem that has been given. The constraints are described as below:

1. Constraints imposed by the power dynamic balance

$$P_t^{PV} + \sum_{v}^{V} P_{t,v}^{EVdisch} + P_t^{buy} = d_t^{sup} + \sum_{r=1}^{R} d_{t,s}^{shift} + \sum_{v=1}^{V} P_{t,v}^{EVcharg} + P_t^{sell} \quad (7)$$

where, P_t^{PV} is the power to be provided by PV plants, d_t^{sup} the supplied essential loads, *and* $d_{t,s}^{shift}$, loads that can be shifted

2. Constraints imposed by variable loads which can be shifted

$$\sum_{t=1}^{T-(L_r-1)} x_{t,r}^{shift} = 1 \quad (8)$$

$$d_{t,s}^{shift} = \sum_{l=1}^{L_r} D_{l,r}^{shift} x_{t-l+1,r}^{shift} \quad (9)$$

with $x_{t,r}^{shift}$ indicating the beginning of shiftable loading and $D_{l,r}^{shift}$ describing the pattern of shiftable loading.

3. EVs demand and supply constraints

$$P_{t,v}^{EVdisch} \leq P_v^{EV\,max} \times SOC_{t-1,v} \quad (10)$$

The supply from or to EV is estimated by using (11), with V denoting the how many EVs are deployed.

$$P_{t,v}^{EV} = \left(\varepsilon P_{t,v}^{EV\,charg} - \frac{P_{t,v}^{EV\,disch}}{\rho} \right) \tag{11}$$

$$N_v SOC_{t,v} = N_v SOC_{t-1,v} + P_{t,v}^{EV} \tag{12}$$

$$SOC_v^{\min} \leq SOC_{t,v} \leq SOC_v^{\max} \tag{13}$$

with SOC denoting the state of charge of the battery, ρ the battery discharging efficiency, and ε the battery recharging efficiency.

4. Aggregator participation constraints

Each aggregator is responsible for determining the minimal amount of power that is allowed to contribute to frequency control, as detailed in (5) and depicted in the flowchart seen in Fig. 3. When the inequality constraint is taken into consideration, the optimal contributed power is estimated as in (14).

$$P_i^a \leq \Delta P_{ji}^0 \leq P_i^{max} \tag{14}$$

In the above equation, ΔP_{ji}^0 indicates the optimal power contribution that needs to be calculated in accordance with Fig. 3.

2.4. Dynamic frequency response analysis with RES integrated

MATLAB Simulink was used as the setting for the development of the model of the Rwandan three-area system. It is expected that all three of these locations are running in parallel at the standard frequency of 50 Hz. The simulation began by taking into account the current power system, and then it compared the results to an estimated model of what the power system will look like in the future after renewable energy sources (RES) have been incorporated and aggregators have participated in the frequency stabilization process. The investigation was carried out after the disruption that had been applied, which had been brought on by the loss of generation of 20 MW at t = 2 s. As can be seen in Fig. 6, the power system is made up of 42 different types of power plants, including hydro, solar, and thermal power plants, all of which are interconnected with one another. These power plants are governed by three distinct control zones, which are referred to as the North zone, the South zone, and the Western zone, respectively. After the overall system inertia constant has been calculated, a frequency response model for the diagram that has been given is next investigated. This model has all of the generators in the same zone and of the same type grouped together as one generator unit.

The electric distribution system is modelled in IPSA+ Power software tool, which is specifically used to analyse the steady-state operating characteristics of power systems with an option including load-flow analysis. The generation mix in the system includes hydropower plants with a total power of 103.16 MW), and diesel-based plants with a total power of 58.8 MW.

There are four PV power plants with a total installed and available capacity of 12.08 MW and 1.9 MW, respectively. Furthermore, the only peat fired plant in the country has a capacity of 15 MW and provides a power of up to 14.25 MW. Lastly, there is also a methane-to-power plant with an installed capacity of 26.4 MW, which was commissioned in December 2015.

Overall, the existing generation plants (including hydro, diesel, methane gas, biomass, and peat-to-power) in Rwanda can provide up to 222.9 MW. The IPSA+ schematic diagram of the network is shown in Fig. 6.

There are a total of 14 different generation substations, as illustrated in Fig. 6, and their installed capacities are listed in Table 1.

Table 1
Installed capacity for the system under study.

Busbar	Power (MW)	Power (MVAr)
KILINDA	27.0000	−6.8748
GIHIRA GEN	1.8000	−0.1799
CAMP BELGE	2.4000	8.6741
GIHIRA	6.9000	7.3416
KIVUWATT	25.0000	4.1503
JABANA MV	7.0000	1.0878
NTARUKA	8.9	−1.1380
JABANA THERMAL	20.0000	−0.1955
RUGEZI S	2.6000	3.5458
GISENYI GEN2	1.3000	0.4539
GIKONDO MV	47.0000	2.1073
MASHYUZA	40.0000	−1.9107
MUKUNGWA1 MV	28	−6.7247
RUKARARA	5	−0.214

As for the load characteristics, the demand for electricity range between 87 and 193 MW with the installed generation presented in Table 1. The minimum power demand has increased from 42.9 MW in 2013 to 12 MW in 2021 while the maximum peak power demand increased from 87.7 MW to 193 MW. It is recognized worldwide that the main electricity demand categories are agriculture, services (or commercial), residential (or households), industrial and transport sectors. However, in some countries such as Rwanda, the consumption by some of these sectors are insignificant in such a way that they are ignored when classifying the demand and some others are split into subcategory for a better management. The electricity demand categories followed the classical categorization until 2008. After 2008, however, the demand categories are classified into normal customers, medium customers, public customers plus the REG consumption. In this study, the demand classification is not taken into consideration, as the needed data is only the connected load at each substation as depicted in Table 2.

After the calculation of the total system inertia has been completed, the frequency control model shown in Fig. 7 is investigated. The investigation assumes approach, all generators operating in the same zone and having the same model are regarded as constituting a single generating unit. Based on the results of the MATLAB Simulink simulation study, a typical Rwandan power system is depicted as a three-area system that integrates hydro, thermal, and solar electricity, all of which are linked together by tie-lines. In order to get other significant network base characteristics, in addition to the data presented in Mudaheranwa et al. (2022), extra calculations and assumptions were undertaken. The obtained values for each parameter are represented in Tables III through Table 5, which are discussed in the subsequent subsections.

2.4.1. A determination of the governor speed regulation, as well as the system stiffness and load damping, and the system synchronizing power coefficient

In a multi-generator network, the analogous generator model representation that is found in Anon (2021a) can be employed if it is assumed that all of the generators work at the same synchronous speed. The equivalent load-damping constant, denoted

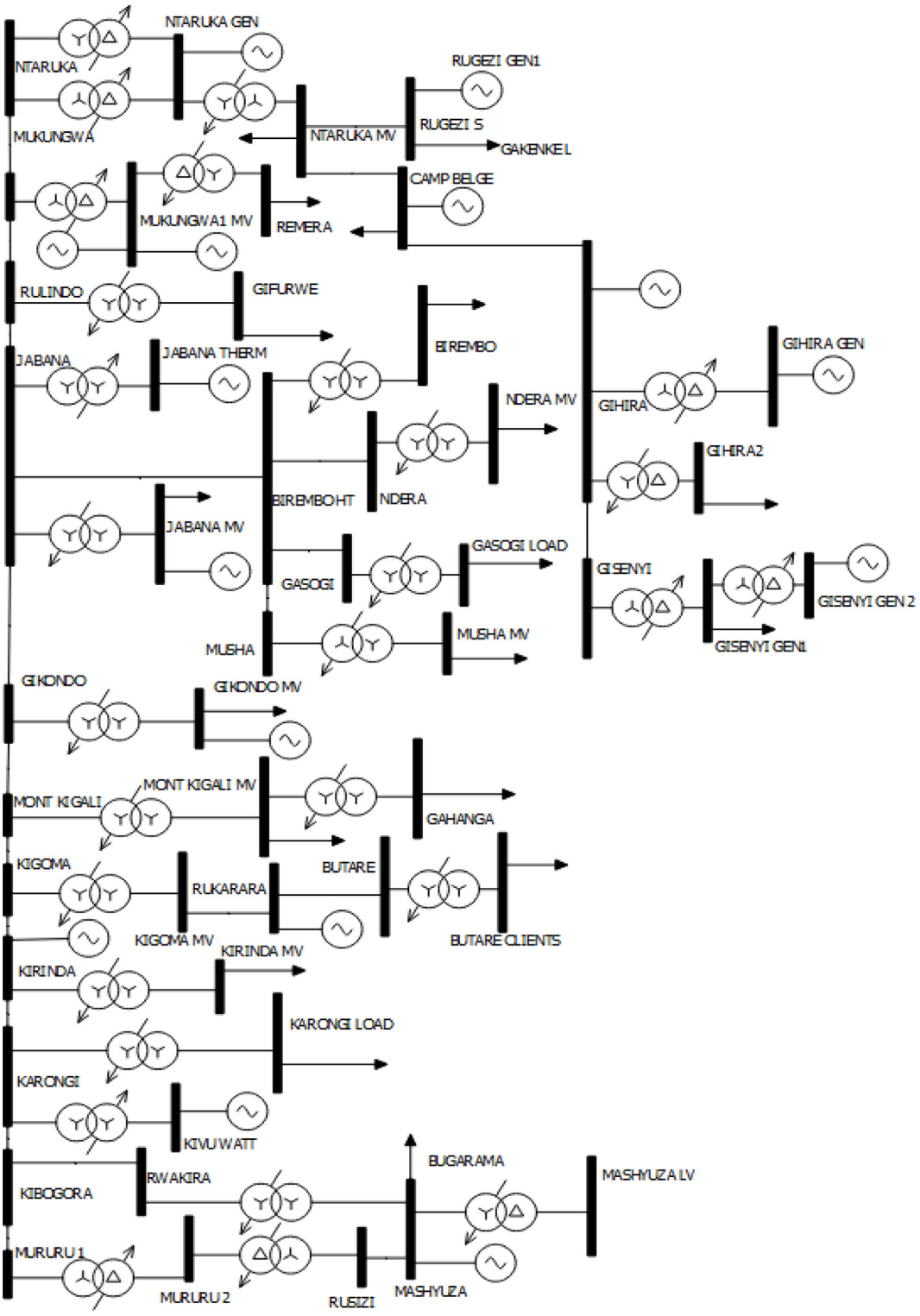

Fig. 6. Modelled network without EVs chargers' deployment.

by (D_{eq}) is determined by the formula given in (15).

$$D_{eq} = \frac{\sum_i^n D_i}{n} \tag{15}$$

With n, the total number of participating generating unit and D_i is the individual load responsiveness that corresponds to the change in frequency for every individual generating unit in turn. In a power system, the combined effect of the droops of all the alternators' speed governors as well as the frequency adaptation characteristics of each load determines the system's power to frequency characteristics. This is because the system as a whole determines the frequency adoption behaviours of all loads. This power to frequency ratio can be used to determine the load damping factor and the governor speed control (Sallam et al., 2015; Anon, 2021a). The load-damping factor is stated as a proportional variations in demand divided by proportional variations in frequency for a system that has n generating units. The steady state frequency variation (Δf_{SS}) following a change in load (ΔP_L)

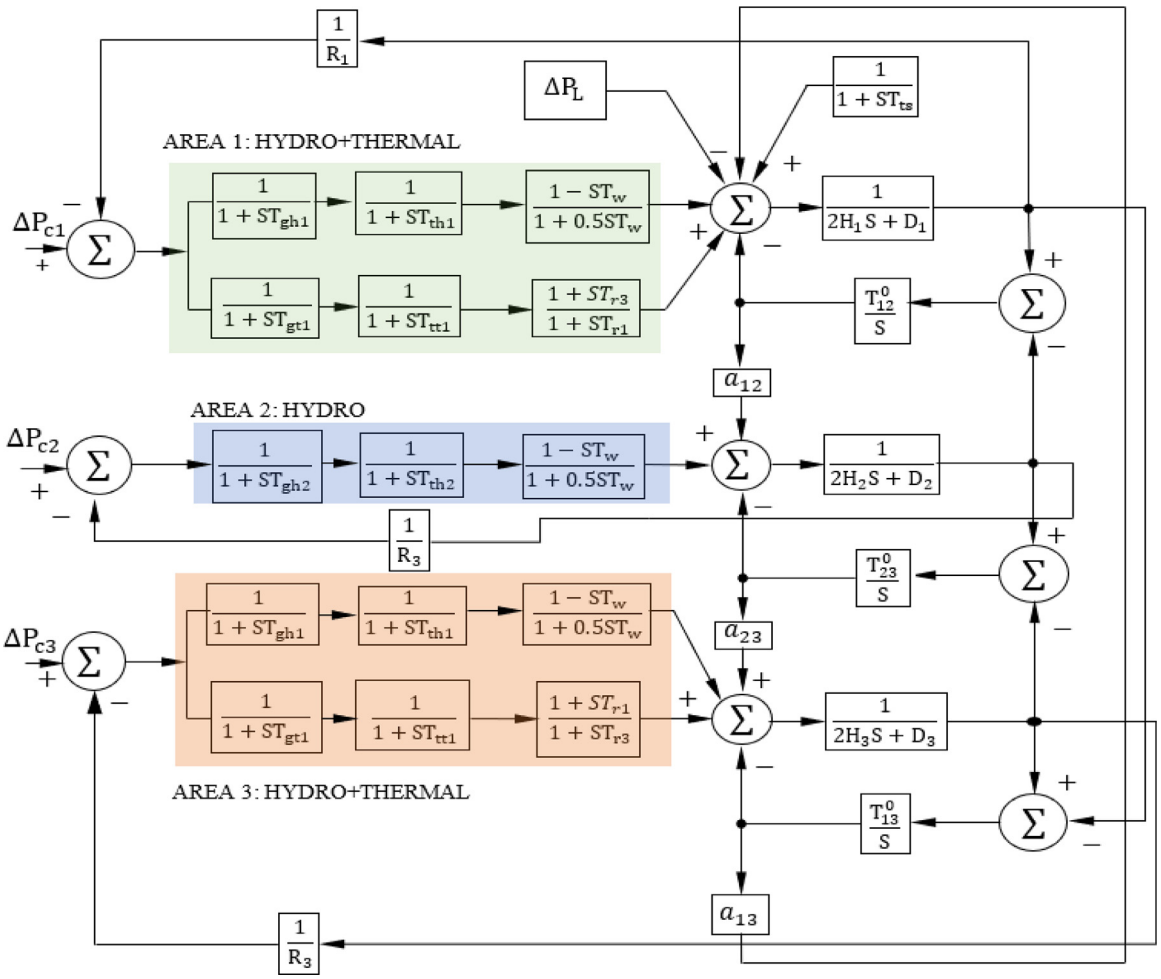

Fig. 7. Dynamic frequency control model showing all three control areas with their integrated power generation technology.

is provided as in (16).

$$\Delta f_{SS} = \frac{-\Delta P_L}{\left(\frac{1}{R_1} + \frac{1}{R_2} + \cdots + \frac{1}{R_n}\right) + D} \tag{16}$$

The individual governor speed regulation is represented by the parameter R_i, in per unit. As a result, the composite frequency dynamics of the grid is determined as in (17).

$$\beta = \frac{1}{R_{eq}} + D \tag{17}$$

Where:

$$R_{eq} = \frac{1}{R_1} + \frac{1}{R_1} + \cdots + \frac{1}{R_n} \tag{18}$$

The stiffness of the system is often denoted by the composite frequency response characteristic denoted by the symbol "," which is commonly stated in MW/Hz. An increase in system load by ΔP_L (at the usual frequency) results in an increase in total generation by ΔP_G due to the action of the governor, and a reduction in total system load by ΔP_D due to the frequency sensitive feature (Sahin, 2020; Moorthi and Aggarwal, 1974; Anon, 2021b,a),

A power system's load damping factor can be calculated using data on load and frequency changes collected over time from the three control regions, as is the case in this study. Table 3 displays the results of the load and frequency change tests. Table 3 also displays the results of the computation for the average of each change, based on the sample of five unique events that were collected from each substation of the three regions. Additionally, the calculated load damping factor is included in Table 3 for each region. The calculated average load damping factor at the North zone is approximately 1.05, while that at the South zone is approximately 1.38, and that at the West zone are approximately 1.10.

The modelled version of the system under investigation includes additional control modes. In this regard, the calculations for both the stiffness of the system and the constant for the governor's speed control are carried out. The constant for regulating the speed of the governor, denoted by "R", and the system stiffness, denoted by (β) can be determined by applying the relationships shown in Fig. 3 of Mudaheranwa et al. (2022). Table 4 presents the results of the calculations made for the values of R and for generating and installed capacity.

As was previously mentioned, the system is a supplementary controlled interconnected network that features three distinct control regions. The dynamic frequency control system in each region of the system shall regulate the interchanged power and its frequency with other existing control areas in order to serve as the foundation for supplemental control (Sallam et al., 2015). As a result, the power transmissions and the reactance readings of the tie-lines are taken into consideration during the analysis of the stated dynamic LFC system model in order to arrive at an estimate of the system's synchronizing power coefficients.

During typical operations, the power on the tie-line that is responsible for the flow of energy from control area 1 to control area 2 ($P_{tie,12}$) is derived from (16).

$$\Delta P_{tie,12} = \frac{|V_1||V_2|}{X_{12}} \cos(\delta_1 - \delta_2)(\Delta\delta_1 - \Delta\delta_2) \tag{19}$$

Table 2
Connected load for each substation.

Busbar	Power (MW)	Power (MVAr)
JABANA MV	11.7	0.1000
GISENYI GEN1	3.5000	0.1000
MASHYUZA	5.4000	0.6300
RUGEZI S	2.0000	0.2000
KARONGI LOAD	26.3	0.0600
NDERA MV	1.2000	0.1000
GASOGI LOAD	10.20000	0.9800
BUTARE CLIENTS	30.5	0.2200
GIFURWE	7.6	0.2000
GIKONDO MV	24.1000	1.1000
KIRINDA MV	3.6000	0.1000
BIREMBO	14.5	0.1000
NTARUKA MV	23.1	0.1000
CAMP BELGE	12.6	0.0700
MUSHA MV	1.5000	0.1000
MONT-KIGALI MV	4.3000	0.9000
REMERA	3.5000	0.1000
GIHIRA 2	5.4000	0.6300
GAHANGA	2.0000	0.2000

Table 3
Estimated load damping factors.

Area	Case	Change in frequency (%)	Change in load (%)	(D_i)
1	1	1.3	1.3	**1.05**
	2	1.14	1.1	
	3	0.32	0.2	
	4	0.36	0.8	
	5	1.56	0.2	
Mean value		**0.7**	**0.664**	
2	1	0.57	0.6	**1.38**
	2	0.8	0.2	
	3	0	0.6	
	4	0.81	0.6	
	5	0.61	0.2	
Mean value		**0.41**	**0.315**	
3	1	0.55	0.51	**1.11**
	2	0.38	0.38	
	3	0.19	0.11	
	4	0.00	0.0	
	5	0.79	0.71	
Mean value		**0.298**	**0.3079**	

Table 4
Estimated R and β coefficients.

Generated power (MW)	Capacity (MW)	Supply change (MW)	R	β
91.01	122.03	25.56	0.051	39.01
90.77	121.73	25.41	0.044	
91.65	121.73	24.69	0.0131	
91.12	121.73	25.14	0.0139	
91.60	121.73	24.73	0.062	
R_{1eq}			**0.0261**	
37.19	40.81	8.81	0.069	28.6
37.31	40.81	8.52	0.1	
37.2	40.81	8.84	0	
36.81	40.81	9.76	0.079	
37.19	40.81	8.91	0.071	
R_{2eq}			**0.0351**	
56.51	62.55	9.65	0.0559	32.9
56.6	62.55	9.50	0.0401	
56.75	62.55	9.26	0.0202	
56.78	62.55	9.21	0	
56.4	62.55	9.82	0.0801	
R_{3eq}			**0.0320**	

Table 5
Computed synchronization power factor.

Control area 'i'	Control area 'j'	Reactance (Ω)	Synchronization factor (T_{ij})
2	3	0.67	0.55
1	3	0.56	0.57
1	2	0.44	0.41

Voltage magnitudes and phase shift

Regions	Rating in voltage (pu)	Phase shift (degrees)
1	0.9821	24.23
2	1.0057	24.82
3	0.985	2.79

The expression $\frac{|V_1||V_2|}{X_{12}}\cos(\delta_1 - \delta_2)$ is specified as the tie-synchronizing power factor (T_{12}), and therefore its power imbalance has the general expression as given by:

$$\Delta P_{tie,12} = T_{12}(\Delta\delta_1 - \Delta\delta_2) \tag{20}$$

In complement to the MATLAB model used to conduct the dynamic frequency control analysis, the Rwandan power system was studied and analysed in IPSA+ Power software. This was accomplished by carrying out a power flow in order to acquire the voltage and phase shift magnitudes and hence determine the power synchronizing coefficient. The voltage magnitude and angle values, along with the synchronizing coefficient that was determined, are presented in

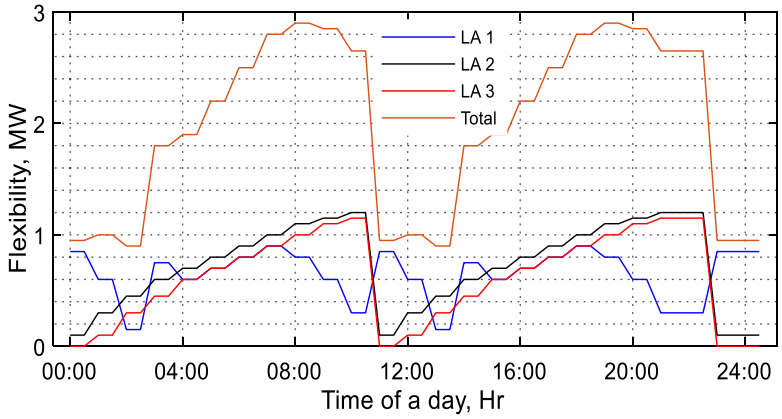

Fig. 8. Predicted available flexibility.

Because the data necessary to compute the governor and turbine time characteristics are not currently accessible, the governor and turbine time constants are chosen according to the guidelines outlined in the technical report (PES-TR1) (Mcgill et al., 2022; Anon, 1973) published by the IEEE Power & Energy Society.

3. Results and discussions

3.1. Aggregators possible contribution

This study takes into account a practical control area that has residential and industrial loads and has the capacity to accommodate one thousand 1000EVs. The source that was used to collect the data and the parameters of the behaviours of EVs in traffic is Ulbig et al. (2014). Mudaheranwa et al. (2020) is the source from which we acquired the data and parameters about the usage behaviours of shiftable loads. The use of historical data was necessary to check the findings of the prediction in order to assess flexibility. On the other hand, because there was a lack of historical data for the region that was the subject of the investigation, the information regarding EV charging was obtained from Udoakah et al. (2019), and the information regarding shiftable load utilization was obtained from Luo et al. (2013). Fig. 8 displays the findings of the flexibility forecast. The purpose of this study is to investigate a region that has three aggregators, each of which is represented by a unique shade in the figure below.

The findings that are provided in Fig. 7 are taken into consideration during the optimization process in order to determine the aggregator's ideal contribution to the dynamic frequency control. The findings are obtained by applying the parameter continuation approach described in Sandels et al. (2014) to optimize with equality and inequality constraints. This allows for the optimization to be performed. Fig. 9 displays the results obtained from carrying out the optimization. The figure illustrates the optimal amount of electricity that an aggregator is able to provide to the grid at an affordable price from either the consumer's side, the grid's side, or the aggregator's side throughout the course of an entire day.

Load aggregators have a responsibility to take into account a variety of criteria, including the satisfaction of consumers, the comfort of power use, and the habits of energy usage. In this context, the load aggregator is obligated to make scheduled provisions in ahead and provide customers with early notification of the preparations. It has already been supposed that the load aggregator has considered the factors of cost optimization when establishing the scheduling plan in order to fulfil the constraints of user delay times and obtain the most cost-effective planning

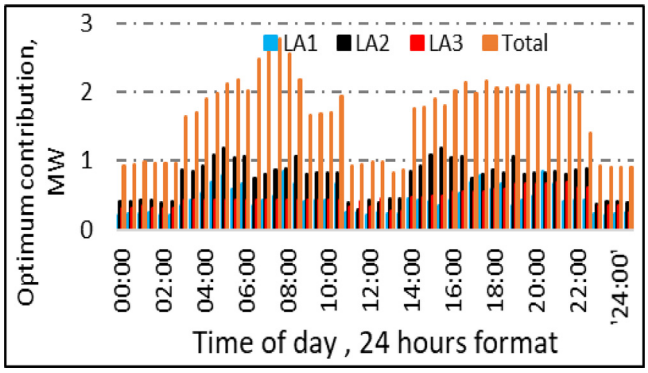

Fig. 9. The amount of power that was contributed by the aggregator after optimization.

combination that is possible. After taking all of this into account, the aggregator calculates how much of a contribution it makes to the frequency regulation. The findings indicate that the analysed region with three aggregators provides the most contribution between the hours of 6:00 and 8:00 in the morning, it provides the least contribution between the hours of 22:00 and 24:00 in the evening.

3.2. Aggregators participation for the stabilization of grid frequency

The MATLAB Simulink toolbox was used to develop the Rwandan three-area control system. The interconnected areas are supposed to operate at a synchronized frequency of 50 Hz, which is the standard. The network was modelled after the disturbance was applied at t = 2 s (loss of generation) and 20 MW was assumed. With this loss of generation, the analysis looks at the Future Energy Scenarios (FESs) of Rwanda's energy system as they are presented in Li and Dankowicz (2022). Estimates of energy demand and production capability through the year 2050 are conducted using the FESs developed in Li and Dankowicz (2022). Three different scenarios for energy usage and electricity production have been defined, taking into consideration a time frame ranging from 2019 to 2050. These scenarios are derived from various social, political, and economic influences, the variety of power generation advanced technology (including renewable energy resources), regional integration, and CO_2 emissions. According to the information presented in Anon (1973), the three distinct possibilities can be broken down into three categories: the basic, medium, and high advancement scenarios. In order to carry out simulations, the projected changes in solar photovoltaic

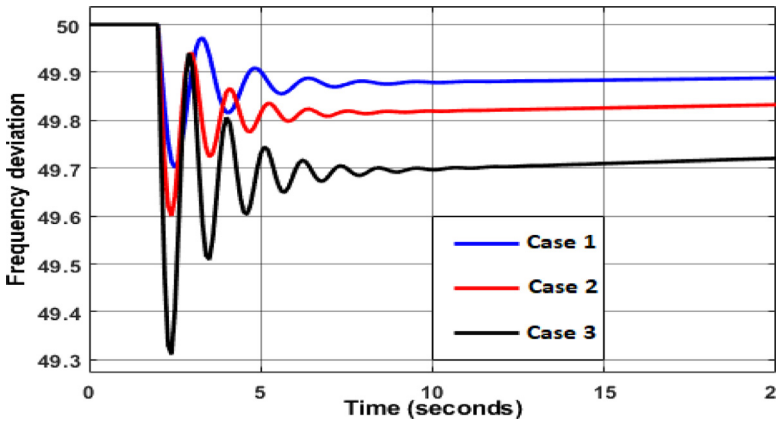

Fig. 10. Frequency variations and restoration in control area 1 with different solar PV penetration.

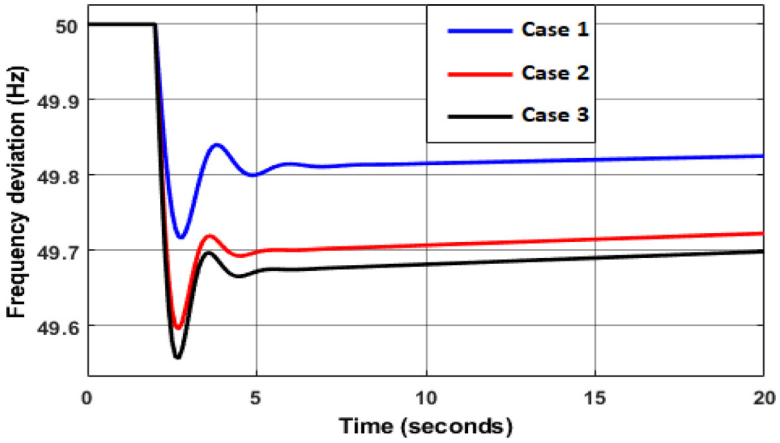

Fig. 11. Frequency variations and restoration in control area 2 with different solar PV penetration.

(PV) uptake that occur during low, medium, and high progressing scenarios are considered.

After considering the results presented in Figs. 7 and 8, the frequency response of the case study is analysed. The proposed Load Frequency control is examined after loading the load control algorithm into the conventional LFC Simulink model

Basic progression scenario

During the analysis, the behaviour of the grid model is investigated with photovoltaic (PV) plants and the participation of the aggregator in the frequency stabilization taken into consideration. Because solar photovoltaic and electricity import do not follow the conventional generation inertia, the inertia of the entire system will be negatively impacted as a result of their integration in the power supply mix. This study considers the solar PV integration estimated in Mudaheranwa et al. (2022) for three different periods namely 2025, 2035, 2050. The estimated solar PV integration for the above mention periods in control area 1 is 21% for the year 2025, 27% for the year 2035, and 30% for the year 2050 in this scenario.

Assuming a loss of generation of 20 MW at t = 2 s, as well as the above-mentioned solar PV integration percentages in the overall generation, it is seen that the frequency in each region falls below the standard value of 50 Hz, as depicted in Fig. 10. However, the results of the simulation show a frequency that appears to be restored to 50 Hz within a very long duration because the results show a frequency of approximately 49.85 Hz after a duration of 12 s. This suggests that the frequency will be restored to 50 Hz within the very long duration. This decrease in frequency is the result of an increase in the provided load as well as an increase in the PV generation that corresponds to that increase. The frequency variations during the entire simulation period in control area 1 with PV integrated is depicted in Fig. 10. This response is shown for the periods 2025, 2035, and 2050.

At 30% PV penetration (in the year 2050), frequency dropped the most because equivalent inertia decreased. As a result, the system operates at below maximum allowable frequency of operation of 49.8 Hz. For 2025 and 2035, the frequency decreased from nominal, but it was still within the power system's safe working limits. To avoid the negative effects of extreme frequency variations, a proper control technique must be used to maintain load-generation balance and safe frequency.

According to simulation results by considering control area 2, 28% PV adoption is the point at which frequency decrease is most pronounced for solar PV plant integration in years 2025,2035 and 2050. As a result, the frequency drop is also lower, but less compared to the frequency drop in control area 1 (Roughly 0.029 Hz difference). Fig. 11 shows the frequency characteristics results in the control area 2 with integrated PV three different scenarios. It is observed that the frequency in controlling zone 2 during the years 2025 and 2035 restores to its set point after roughly t = 3s just after perturbation. On the other hand, its same situation occurred in control area 2 when the year 2050 was taken into consideration after approximately t = 6s. It can be shown that the synchronization in this control area happened much more quickly in 2035 and 2050 compared to 2025. However, because of the decrease in the inertia constant, in year 2035 and 2050, both display a larger frequency drop in conjunction with a lower working frequency.

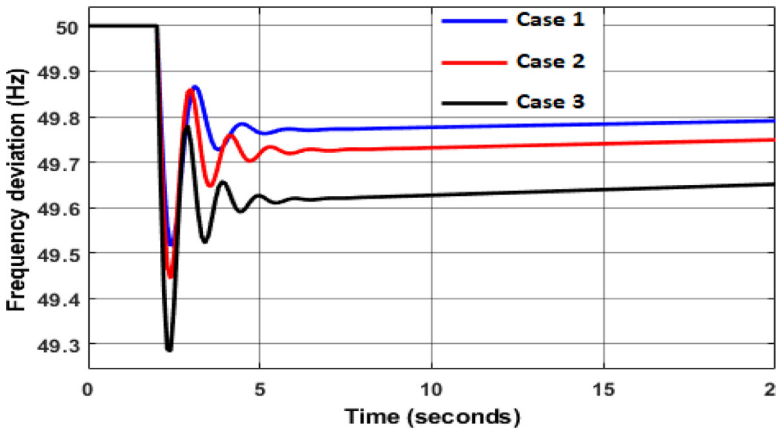

Fig. 12. Frequency variations and restoration in control area 3.

Fig. 12 presents a visual representation of the frequency transients for the control area 3. This number makes it abundantly evident that the maximum overshoot will be somewhere in the neighbourhood of 0.478 Hz in the year 2025, 0.541 Hz in 2035, and 0.72 Hz in 2050; this is equivalent to 0.956, 1.09, and 1.42 percent in frequency drop, respectively. In addition, the amount of time it will take for the frequency to stabilize following a step alteration in generation is somewhere around five and six seconds.

It is observed to have the largest value for maximum frequency drop for the year 2050, which indicates that the decrease in inertia forces the frequency to go less than its operational value. This occurs with a penetration of 16 percent for photovoltaic systems. Because of this, a suitable control technique needs to be utilized to assist in the demand–supply balancing so that the frequency may be maintained at a level that is both efficient and safe for performance. This is necessary in order to avoid the unfavourable consequences of a high frequency variations. After considering the participation of aggregator for the stabilization of frequency, simulation results shown in Fig. 13 shows the frequency response for each year.

When compared to the frequency responses that were seen prior to taking into account the participation of the aggregators, the findings that were obtained after taking into account the suggested method reveal a frequency that has been restored to the normal for all years. When there is a PV generation integrated, the primary objective of aggregator in this work is to exercise control and regulation over the frequency of the system. The initial simulation results demonstrate that the aggregator participation lessens the decrease in the system frequency while simultaneously lowering the amount of undershoot, as can be shown in Fig. 7. The frequency at which the system operates is between 49. 664 Hz and 49.81 Hz for all three control areas when the aggregator participation method is not present in the network; however, when the method is introduced, the frequency at which the system operates increases to the normal which is 50 Hz in this case.

The utilization of aggregator grid frequency stabilization within the system to supplement the PV generation and to furnish a prompter reaction within the power system is the root cause of the increase in frequency that has been seen.

Medium progression scenario

The decreasing inertia constant observed in this scenario is a result of renewable technology becoming more widely adopted. The PV solar installed capacity, for example, was expected to be 25 percent, 32 percent, and 37 percent from the years 2025 to 2050, respectively. As consequence, a higher drop in frequency is also observed. Fig. 14 show the estimated frequency response characteristics before the aggregators are considered as contributors to the frequency stabilization.

The findings presented in Fig. 13 demonstrate that there is an increase in frequency deviation as a result of a greater percentage of renewable energy resources present within the system. As PV integration increases, peak oscillations and settling delays also increase, whereas there are some specific frequency dips to lower levels than the normal frequency range. System frequency oscillations (see bottom findings of Fig. 14 left side) are larger in 2050 because of a continued adoption in renewables, while for 2025, because there are fewer PV systems in operation, the frequency variations in the system are at their lowest.

When the contribution of the aggregator is taken into consideration, the findings demonstrate that even though the frequency decreases, it quickly returns to the usual operating limit and stabilizes itself there. As can be seen on the right-hand side of Fig. 14, when the participation of the aggregators is taken into account, the maximum decrease in frequency is observed is in case three, where it drops to 47.5 Hz. However, as a result of the impact of the proposed method, the frequency returns to 50 Hz, whereas it returns to 49.5 Hz when there is no contribution from the aggregators.

High progression scenario

In contrast to the results of other progression scenarios, the simulation carried out using this scenario reveals in Fig. 15 that each control area experiences a higher peak below the frequency at which it is running. In addition, by the year 2050, the system will have seen larger frequency variations and will have moved closer to a state of instability due to the fact that the time it takes for the system to restore itself will be greater than 20 s. To clarify, the computed value of the inertia constant has dropped more precipitously as the share of renewable sources in total energy production has grown at the high rate (from around 7.2 s to 3.83 s). It is evident that the trajectory of deviations and transient response is practically comparable in 2025 and the year 2035. Additionally, the fluctuates in frequency variations that are detected at each time instant are nearly similar in control regions 1 and 3, and this similarity can be related to the connectivity and functioning of thermal power generation (see Fig. 15).

The analysis showed, when the contribution of the aggregator is taken into account, that even though the frequency drops, it quickly returns to the typical working limit and stabilizes itself there, despite the fact that it was initially lower. When the participation of the aggregators is taken into account, as can be seen on the right-hand side of Fig. 15, the scenario in which the frequency drops to its lowest point, which is 49.2 Hz, is the one in

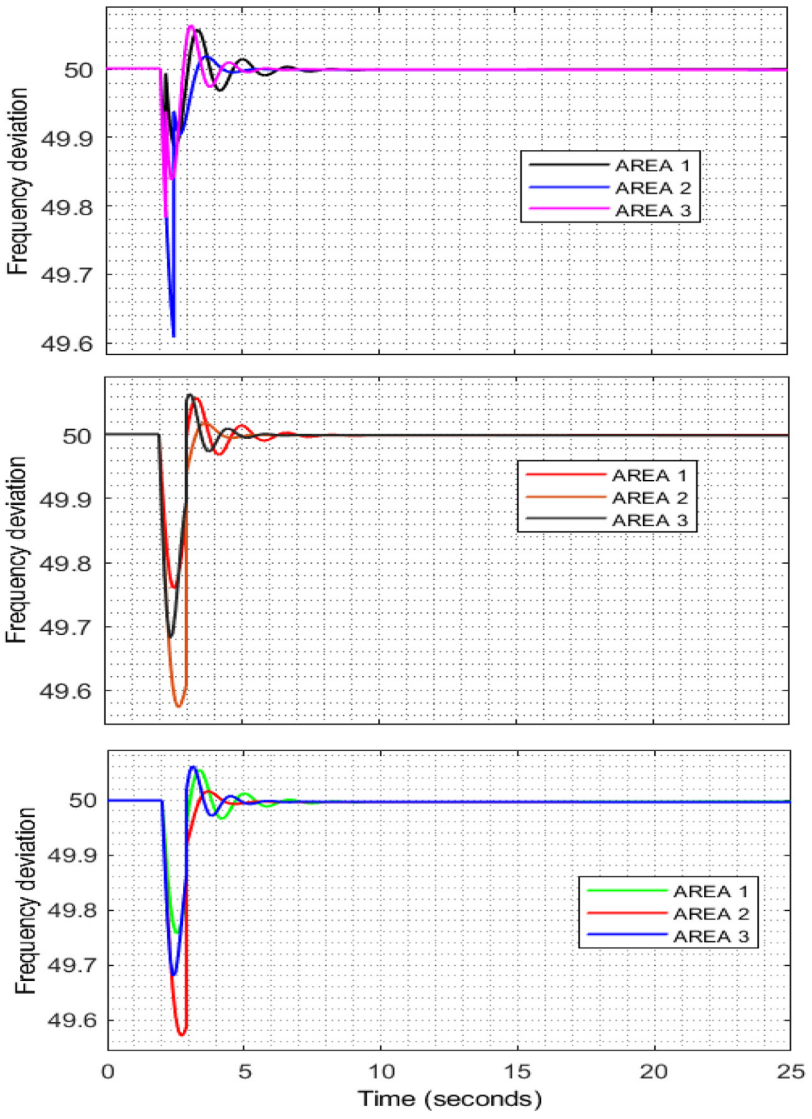

Fig. 13. Frequency response after considering aggregator participation for the year 2025 (top), 2035 (middle), 2050 (bottom).

which the biggest fall in frequency is recorded. The frequency, on the other hand, returns to 50 Hz as a consequence of the impact of the suggested technique, whereas it returns to 49.5 Hz when there is no contribution from the aggregators (see Fig. 15, left).

To visualize the contribution of the aggregators in each control area, this study assumes that the loss of generation happens sometime in the morning, mid-day, and at one instant of time in the night. The amount of power that is contributed by each aggregator in each location is presented in Fig. 16.

With the loss of generation events, the aggregators contribute mainly for the morning event with a contribution of about 4MW followed by the night event with the contribution of approximately 3.5MW. This means that customers in the morning and night are consuming higher energy. However, results show that when consumption is well managed by aggregators the power that could have been consumed by uncontrolled loads is virtually sent back to the grid and therefore, contributes to the grid stability.

As for the data for the usage behaviours of different type of loads from looking at the case by case of the load under consideration, the study considers first the household characteristics, as a basic reference. This work considers the household characteristics based on a typical house consumption data in the Sub-Saharan Africa region in which the case study is located at.

Table 6
Power demand of a typical household appliance in sub-Saharan Africa (Adkins et al., 2012).

Appliances	Power (W)	Appliance	Power (W)
Fluorescent lamp	40	Air conditioner	2000
Washing machine	380	Water heater	1100
Microwave oven	900	Television	180
Iron	1000	Computer	50
Refrigerator	220	Cooker	500

Table 6 lists some of the appliances found in a typical home considered for the case study.

The working behaviours of the appliances are estimated in order to predict the possible flexibility that these appliances can provide. For example, the working condition of the refrigerator is very consistent, and it spends each of its 24 operating hours alternating between the work mode and the standby mode. The

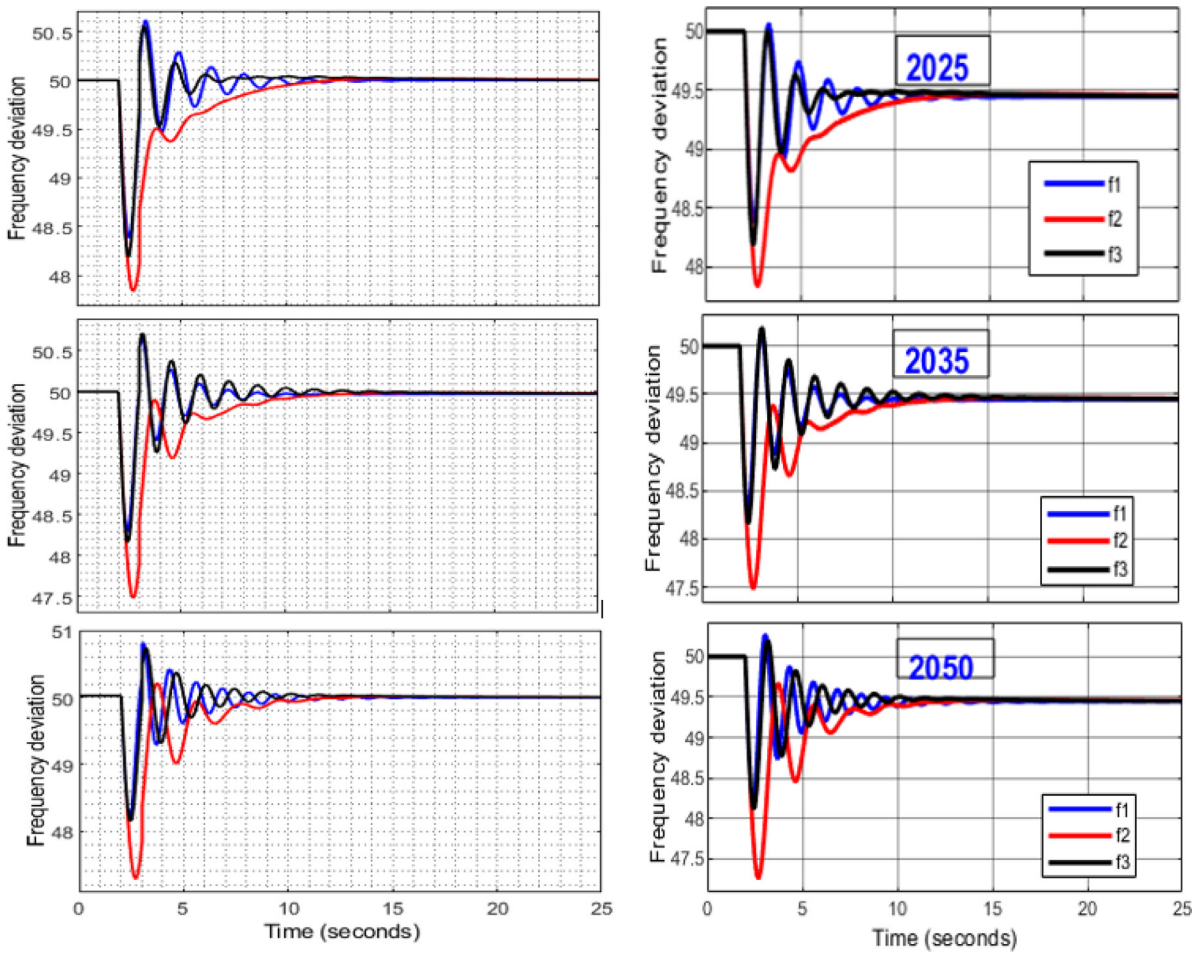

Fig. 14. Frequency response in all three control areas (right: before considering the aggregator participation, left: after considering the aggregator participation) for medium progression.

refrigerator has a reasonably long-running operation mode during the hours of 6:50 and 7:20, 10:40 and 11:20, and 17:40 and 18:10 respectively.

Due to the weather condition, which is nearly the same across the whole Sub-Saharan Africa, the air conditioner is switched on from 0:00 to 4:00, from 12:10 to 13:50, and from 19:30 to 24:00. Fig. 17 depicts the operating probability of six typical home appliances based on their electricity usage patterns.

To estimate the day-ahead and real-time cost for a single day this study refers to the electricity tariffs in Rwanda. As of January 2021, the Rwanda Utilities Regulatory Authority (RURA) has announced new electricity tariffs that are different than the ones introduced in 2018. This study considers the end-user electricity prices that were reviewed in order to meet the required operational and investment expenditures for the utility. The electricity tariffs adopted from Rwanda Utilities Regulatory Authority (2022) are presented in Table 7. The presented electricity tariffs are obtained by calculating several data points at various levels of electricity consumption. This means that the end user pays the electricity based on the maximum consumption per month (based on different consumption blocks). To estimate any cost of electricity at any time of a day, this study considers the disaggregation of the presented tariffs where it is necessary.

The annual costs for the three scenarios that were mentioned earlier can be seen in Table 8. These costs are broken down into two categories: those that occur when there is no Aggregator participation and those that occur when Aggregator participation is considered.

The most important things to notice are: (1) Participation of an aggregator lowers costs, and in all three scenarios, the total costs are lowest when an aggregator is taken into account. It makes the total cost of the Basic progression scenario 11% lower than the "No Aggregator Participation" case, 11% lower for the medium progression scenario, and 16% lower for the high progression scenario. So, using Aggregator participation is a good way to take advantage of how prices change in real time.

3.3. Comparison of the presented work with existing solutions

This section compares the presented work with existing solutions based on different controller types, soft computing approaches, time-domain analysis, and the performance index.

Time-domain study compares parameters such as undershooting, settling time of different area frequency deviation (ΔF1, ΔF2), and tie-line power fluctuation (P_{tie}). In conventional power systems, it is realized that the use of renewable energy sources such as solar photovoltaics and wind increases system performance. However, to stabilize the system and connect power for a single and multiple-area power system, the only microgrid powered by renewable energy requires advanced control and soft computing approaches. Consequently, the application of separate category-specific controllers and soft computing techniques has been discussed.

The works with the Pappachen and Peer Fathima (2021), Rahman et al. (2020), Xi et al. (2020b), as well as Veerasamy et al. (2022), are taken into consideration. Both describe a two-area power system with various traditional energy resources,

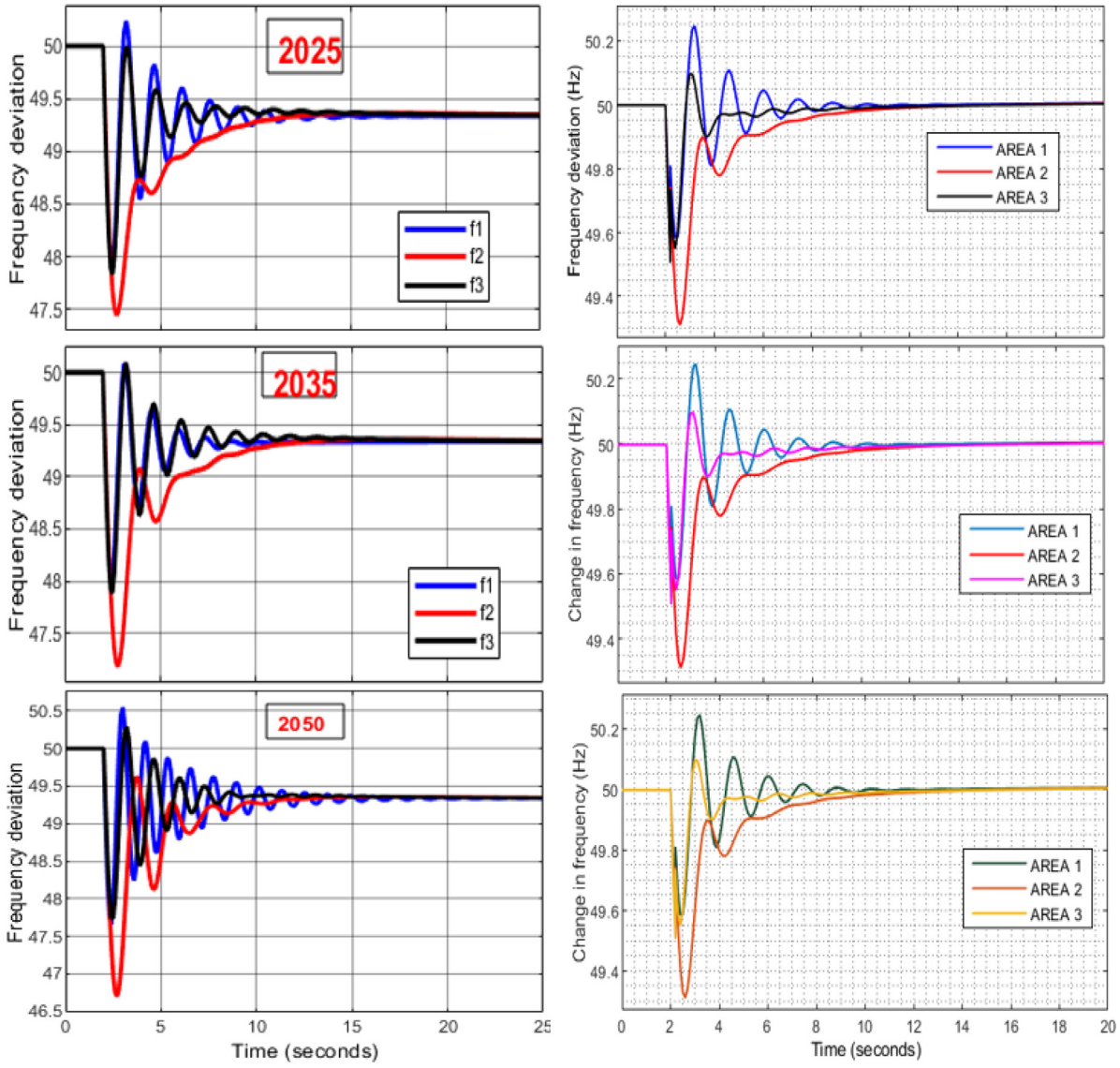

Fig. 15. Frequency response in all three control areas for (left: before considering the aggregator participation, right: after considering the aggregator participation) for high progression.

and Veerasamy et al. (2022) is thought of as a two-area system with nonlinearities such as generation rate constraint (GRC) and governor dead band (GDB). Both of these systems have been studied.

According to Pappachen and Peer Fathima (2021), the transient performance parameter undershoots, overshoots, and settling time of the Adaptive-Neuro-Fuzzy-Inference System (ANFIS) controller are lower than those of the PI and fuzzy logic controllers. Therefore, a system equipped with an ANFIS controller is more stable and provides a faster response to settling than one equipped with a PI or fuzzy controller.

A system with PID, and tilted integral derivative (TID), are compared once more in Xi et al. (2020b), and it is discovered from Table 9 that a system with an TID controller has superior dynamic achievement than a system with a PID, controller. Based on the information presented in Table 9, we are able to draw the conclusion that the energetic performance of the power system containing a Generalized Hopfield Neural Network based self-adaptive Proportional–Integral–Derivative (GHNN-PID) controller is quicker than the performance of the I controller, the PID controller, and the Fuzzy PI controller. However, when the aggregator participation is considered, the system performance is more improved as the settling time, frequency deviation, and Tie-line power fluctuations are decreased as shown in Table 9.

The articles Francis and Chidambaram (2019), Khadanga et al. (2022), Singh et al. (2020), as well as Barakat et al. (2022), are used as references for comparative analyses based on overshoot, undershoot, and settling time. Table 10 provides the data for this research. The Automatic Generation Control (AGC) of multiple-area, multiple-source power systems are examined in Francis and Chidambaram (2019), Singh et al. (2020), whereas the AGC of a two-area power system is considered in Barakat et al. (2022). Conventional PI controller is adjusted in Francis and Chidambaram (2019) using an alternative algorithm such as genetic algorithm (GA)/ Bacterial Foraging Optimization Algorithm (BFOA)/ Differential evolution (DE)/DE-Fuzzy and hybrid DE and PS (HDEPS) fuzzy. Where PS stands as Particle Swarm.

It can be observed that the HDEPS fuzzy PI controller has better system achievement than other control strategies in terms of minimal settling times in frequency and tie lines power deviation. Results show 2.2, 2, and 3.2 s for (ΔF_1, ΔF_2, ΔP_{tie}), as indicated in Table 10. Table 10 in the reference document (Singh et al., 2020) provides an indication of the transient specifications of the dynamic response utilizing PID controllers.

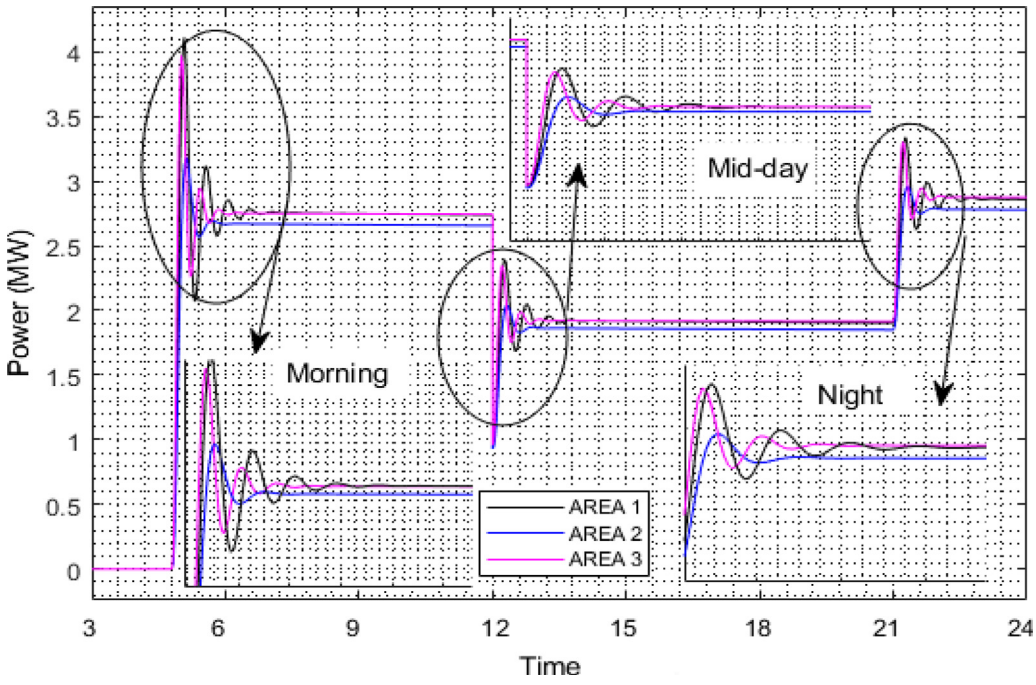

Fig. 16. The power deviation response of aggregators following a loss of generation at three distinct times during the day.

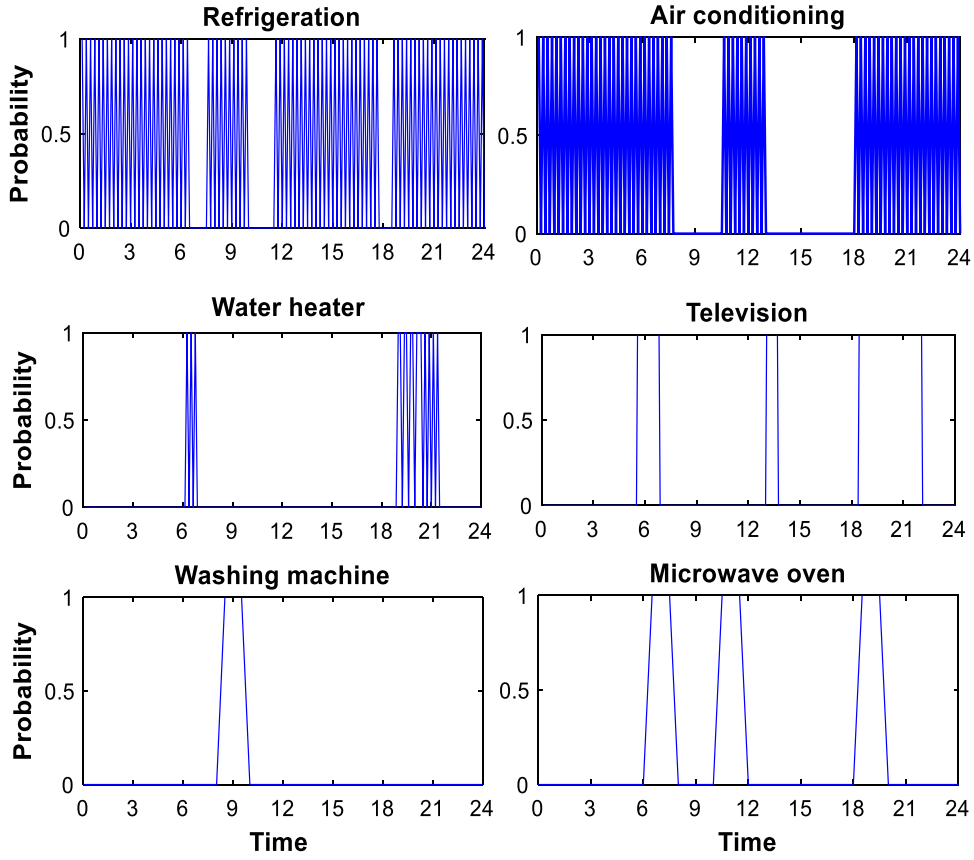

Fig. 17. Estimated consumption characteristics of household appliances.

It is possible to draw the conclusion that when SOS-PID controllers are utilized, the values of overshoot, undershoot, and settling time are reduced to a greater extent than when other controllers are utilized. According to the findings of Khadanga et al. (2022), utilizing an ICA-PID controller rather than a GA-PID controller will result in the tie-line power, frequency deviations, and change in generation being stabilized at steady-state with a shorter settling time and less oscillation. This is the prediction. The performance index undershoots and the settling time of a PI controller that has been tweaked using GA/Fuzzy are offered

Table 7
Electricity end-user tariffs as of January 2021 (Rwanda Utilities Regulatory Authority, 2022).

Customer	Consumption block	Tariff (FRW/kWh)
Residential	≤ 15 kWh per month	89
	]15–50] kWh per month	212
	>50 kWh/per month	249
Non-Residential	≤ 100 kWh/per month	227
	>100 kWh/per month	255
WTP&WPS	all	126
Telecom towers		201
Hotels		157
Health Facilities		186
Broadcasters		192
Small industries ≤ 22000kWh/Year		134
Medium industries]22000–66000] kWh/year		103
Large industries >660 000 kWh/year		94
Data centres		179

Table 8
Total yearly purchased energy cumulative cost in FRW.

	With no Aggregator	With Aggregator	Cost reduction in %
Basic progression	432,764,000	384,032,000	12
Medium progression	411,059,000	364,220,000	11
High progression	400,016,000	335,339,000	16

Table 9
Comparative analysis of the transient performance parameters of different LFC approaches with presented work.

Reference	System configuration	Used controller	Undershoot in Hz for ΔF and in MW for ΔP_{tie}			Overshoot in Hz for ΔF and in MW for ΔP_{tie}			Settling time in seconds		
			ΔF_1	ΔF_2	ΔP_{tie}	ΔF_1	ΔF_2	ΔP_{tie}	ΔF_1	ΔF_2	ΔP_{tie}
(Pappachen and Peer Fathima, 2021; Rahman et al., 2020)	LFC in deregulated power system	Conventional PI	2.2	1.8	35.2	1.4	1.0	15.8	4.8	4.2	5.6
		Fuzzy Logic	1.4	1.2	32.6	1.0	0.7	14.7	3.6	2.8	4.2
		ANFIS	1.3	1.2	28.2	0.9	0.7	12.7	3.6	5.6	5.6
(Xi et al., 2020b)	Interconnected power system	PI D	1.2	1.4	24.9	0.8	0.7	11.2	2.4	2.8	2.8
		TID	0.8	1.6	21.4	0.5	0.9	9.6	4.8	5.6	5.6
(Veerasamy et al., 2022)	Dynamic Interconnected Power System	I Controller	0.5	1.9	17.9	0.3	1.0	8.1	2.4	5.6	8.4
		PID controller	0.6	0.5	14.4	0.4	0.3	6.5	4.8	4.2	2.8
		Fuzzy PI	0.7	0.3	10.9	0.5	0.1	4.9	7.2	4.2	2.8
		GHNN PID	0.4	0.5	7.3	0.3	0.3	3.3	2.4	2.8	5.6
	Presented work	Aggregator participation	0.15	0.12	1.07	0.1	0.11	0.48	1	1	1

once more in Barakat et al. (2022). According to the findings presented in Table 10, it is hypothesized that the power system utilizing Fuzzy PI will have superior dynamic performance than that of GA-PI as a result of lower values of undershoot and settling time. Therefore, it was discovered that the resilience of AGC with Fuzzy-PI controller against random load variations was superior to that of GA-PI controller in this case.

4. Conclusion

In this study, a Load Frequency Control framework based on aggregators is developed to improve the frequency response of the power system. It was demonstrated that the aggregator is capable of forecasting available flexibility for the day ahead contributing to the frequency control process. Results show that it is

Table 10
Transient performance parameters of the PI, Fuzzy PI, and PID controllers considering different algorithms compared with presented work.

Reference	System configuration	Used controller	Undershoot in Hz for ΔF and in MW for ΔP_{tie}			Overshoot in Hz			Settling time in seconds		
			ΔF_1	ΔF_2	ΔP_{tie}	ΔF_1	ΔF_2	ΔP_{tie}	ΔF_1	ΔF_2	ΔP_{tie}
(Francis and Chidambaram, 2019)	Interconnected power system	Conventional PI	1.8	1.60	32.00	1.3	0.88	14.4	4	3	4
		PI with GA	1.2	1.10	29.60	0.9	0.61	13.32	3	2	3
		PI with BFOA	1.1	1.10	25.60	0.8	0.61	11.52	3	4	4
		PI with DE	1	1.23	22.67	0.7	0.68	10.2	2	2	2
		Fuzzy PI with DE	0.65	1.48	19.47	0.5	0.82	8.76	4	4	4
		Fuzzy PI with HDEPS	0.4	1.73	16.27	0.3	0.95	7.32	2.2	2	3.2
(Khadanga et al., 2022)	Interconnected power system	PID with SOS	0.5	0.42	13.07	0.4	0.23	5.88	4	3	2
		PID with ABC	0.6	0.23	9.87	0.4	0.13	4.44	6	3	2
		PID with PSO	0.35	0.48	6.67	0.3	0.27	3	2	2	4
(Singh et al., 2020)	Restructured power system	PID with ICA	0.6	0.73	4.27	0.4	0.40	1.92	2	4	3
		PID with GA	0.85	0.77	3.36	0.6	0.42	1.512	2	2	3
(Barakat et al., 2022)	LFC of 3 areas power system	PI with GA	0.65	0.52	5.07	0.5	0.28	2.28		4	2
		Fuzzy with GA	0.4	0.47	3.47	0.3	0.26	1.56		6	3
	Presented work	Aggregator participation	0.15	0.12	1.07	0.1	0.11	0.48	1	1	1

possible to use DR technology to stabilize the grid frequency. The largest contribution was obtained between 06:00 and 8:00 for the examined area with three aggregators, and the smallest contribution was obtained between 22:00 and 24:00. By considering the whole power system, the findings demonstrate that even though the frequency decreases, it quickly returns to the usual operating limit and stabilizes itself back to the normal operating limits of 50 Hz as a result of the aggregator participation in the process of grid frequency stabilization.

As for the cost analysis, It has been demonstrated that including an aggregator in demand response activities results in cost reductions. According to the findings, the overall expenses are brought down to their lowest point in all three scenarios if an aggregator is taken into consideration. As a result, the overall cost of the basic progression scenario is 11% lower than it would have been in the "No Aggregator Participation" case; the total cost of the medium progression scenario is 11% lower; and the total cost of the high progression scenario is 16% lower. Therefore, taking advantage of the way prices fluctuate in real time is best accomplished through the use of Aggregator participation.

The following suggestions for the probable path to future works could be helpful in improving the research findings and offering interesting research subjects for future research work.

- Software development and experiment-based analysis to study the load aggregator participation in the stabilization of grid frequency
- Market model design based on the conventional load frequency control and the participation of the proposed load aggregator in ancillary services market.
- Frequency response studies using a larger test system and a variety of disturbances and operating conditions.
- Propose diverse mitigate measures for example using storage.

CRediT authorship contribution statement

Emmanuel Mudaheranwa: Conceptualization, Methodology, Software, Data curation, Writing – original draft. **Hassan Berkem Sonder:** Reviewing and editing. **Ye-Obong Udoakah:** Reviewing and editing. **Liana Cipcigan:** Supervision. **Carlos E. Ugalde-Loo:** Supervision.

Declaration of competing interest

The authors declare that they have no known competing financial interests or personal relationships that could have appeared to influence the work reported in this paper.

Data availability

Data will be made available on request.

Acknowledgements

The authors would like to use this opportunity to extend their heartfelt appreciation to the Energy Group in Rwanda for supplying the information that was required. Of addition, the authors would like to express their gratitude to the Commonwealth Scholarship Commission in the United Kingdom for providing sponsorship. Also, authors express their gratitude to DTE Network+, funded by EPSRC, UK, grant reference EP/S032053/1 for supporting this research

References

Adkins, E., Oppelstrup, K., Modi, V., 2012. Rural household energy consumption in the millennium villages in sub-saharan africa. Energy Sustain. Dev. 16 (3), 249–259. http://dx.doi.org/10.1016/J.ESD.2012.04.003.

Agostini, C.A., Armijo, F.A., Silva, C., Nasirov, S., 2021. The role of frequency regulation remuneration schemes in an energy matrix with high penetration of renewable energy. Renew. Energy 171, 1097–1114. http://dx.doi.org/10.1016/j.renene.2021.02.167.

Ahmed, E.M., Mohamed, E.A., Elmelegi, A., Aly, M., Elbaksawi, O., 2021. Optimum modified fractional order controller for future electric vehicles and renewable energy-based interconnected power systems. IEEE Access 9, 29993–30010. http://dx.doi.org/10.1109/ACCESS.2021.3058521.

Angel, S., Mansueti, L., 2009. Customer incentives for energy efficiency through electric and natural gas rate design a resource of the national action plan for energy efficiency. [Online]. Available: www.epa.gov/eeactionplan.

Anon, 1973. Dynamic models for steam and hydro turbines in power system studies. IEEE Trans. Power Appar. Syst. PAS-92 (6), 1904–1915. http://dx.doi.org/10.1109/TPAS.1973.293570.

Anon, 2009. Day-ahead demand response program manual.

Anon, 2011. Smart grid system report 2010 smart grid system report.

Anon, 2021a. Modern power system analysis, 4th edn by kothari-paperback – 2011. (sku:9780071077750). https://biblio.co.uk/book/modern-powersystemanalysis-4th-edn/d/1267333784 (Accessed 26 October 2021).

Anon, 2021b. [PDF]Power system analysis. semantic scholar. https://www.semanticscholar.org/paper/Power-System-Analysis-Saadat/59adb3efdbe9956f9950b90b41bfbc81d1c4082c (Accessed 31 May 2021).

Anon, 2022a. Load serving entities — Descriptive information - energy i-spark. https://ei-spark.lbl.gov/power-markets/load-serving-entities/info/ (Accessed 01 June 2022).

Anon, 2022b. Review and prospect of distribution network planning research considering access of flexible load. [Online] https://o.cnki.net/barnew/download (Accessed 04 June 2022).

Arya, Y., 2020. Effect of electric vehicles on load frequency control in interconnected thermal and hydrothermal power systems utilising CF-FOIDF controller. IET Gener. Transm. Distrib. 14, 2666–2675. http://dx.doi.org/10.1049/ietgtd.2019.1217.

Barakat, M., Donkol, A., Salama, G.M., Hamed, H.F., 2022. Optimal design of fuzzy plus fraction-order-proportional-integral-derivative controller for automatic generation control of a photovoltaic–reheat thermal interconnected power system. Process Integr. Optim. Sustain. 6 (4), 883–900.

Burger, S., Chaves-Ávila, J.P., Batlle, C., Pérez-Arriaga, I.J., 2017. A review of the value of aggregators in electricity systems. Renew. Sustain. Energy Rev. 77, 395–405. http://dx.doi.org/10.1016/j.rser.2017.04.014.

Bussieck, M., Meeraus, A., 2002. General algebraic modeling system. [Online]. Available: www.gamsworld.org.

Coppl, D.A., Nguyen2, T.A., Byrne, R.H., 2020. Real-time Dispatching for Energy Aggregators with Energy Storage and Stochastic Renewable Generation in Markets.

Das, C.K., Mahmoud, T.S., Bass, O., Muyeen, S.M., Kothapalli, G., Baniasadi, A., Mousavi, N., 2020. Optimal sizing of a utility-scale energy storage system in transmission networks to improve frequency response. J. Energy Storage 29, 101315. http://dx.doi.org/10.1016/j.est.2020.101315.

Datta, U., Kalam, A., Shi, J., 2019. The relevance of large-scale battery energy storage (BES) application in providing primary frequency control with increased wind energy penetration. J. Energy Storage 23, 9–18. http://dx.doi.org/10.1016/j.est.2019.02.013.

Debbarma, S., Dutta, A., 2017. Utilizing electric vehicles for LFC in restructured power systems using fractional order controller. IEEE Trans. Smart Grid. 8, 2554–2564. http://dx.doi.org/10.1109/TSG.2016.2527821.

Dehghanpour, K., Afsharnia, S., 2015. Electrical demand side contribution to frequency control in power systems: A review on technical aspects. Renew. Sustain. Energy Rev. 41, 1267–1276.

Francis, R., Chidambaram, I.A., 2019. Optimized PI + load – frequency controller using BWNN approach for an interconnected reheat power system with RFB and hydrogen electrolyser units. Int. J. Electr. Power Energy Syst. 67, 381–392.

Gholian, H.A., 2016. Optimal industrial load control in smart grid. IEEE Trans. Smart Grid 7 (5), 2305–2316.

Hadi, Saadat, 1999. Power system analysis.

Hassanzadeh, M.E., Nayeripour, M., Hasanvand, S., Waffenschmidt, E., 2020. Decentralized control strategy to improve dynamic performance of micro-grid and reduce regional interactions using BESS in the presence of renewable energy resources. J. Energy Storage 31, 101520. http://dx.doi.org/10.1016/j.est.2020.101520.

Joung, K.W., Kim, T., Park, J.W., 2019. Decoupled frequency and voltage control for stand-alone microgrid with high renewable penetration. IEEE Trans. Ind. Appl. 55, 122–133. http://dx.doi.org/10.1109/TIA.2018.2866262.

Kerdphol, T., Watanabe, M., Hongesombut, K., Mitani, Y., 2019. Self-adaptive virtual inertia control-based fuzzy logic to improve frequency stability of microgrid with high renewable penetration. IEEE Access 7, 76071–76083. http://dx.doi.org/10.1109/ACCESS.2019.2920886.

Khadanga, R.K., Kumar, A., Panda, S., 2022. A modified grey wolf optimization with cuckoo search algorithm for load frequency controller design of hybrid power system. Appl. Soft Comput. 124, 109011.

Koch, S., 2015. Assessment of revenue potentials of ancillary service provision by flexible unit portfolios. In: Energy Storage for Smart Grids: Planning and Operation for Renewable and Variable Energy Resources (VERs). Elsevier Inc., pp. 35–66, doi: 10.1016.

Kumar, D., Bhushan, R., Chatterjee, K., 2018. Improving the dynamic response of frequency and power in a wind integrated power system by optimal design of compensated superconducting magnetic energy storage. Int. J.Gren Energy 15, 208–221. http://dx.doi.org/10.1080/15435075.2018.1434524.

Latif, A., Paul, M., Das, D.C., Suhail Hussain, S.M., Ustun, T.S., 2020. Price based demand response for optimal frequency stabilization in orc solar thermal based isolated hybrid microgrid under salp swarm technique. Electronics (Switzerland) 9 (12), 1–16.

Li, M., Dankowicz, H., 2022. Optimization with equality and inequality constraints using parameter continuation. Appl. Math. Comput. 375, 125058.

Luo, Z., Hu, Z., Song, Y., Xu, Z., Lu, H., 2013. Optimal coordination of plugin electric vehicles in power grids with cost–benefit analysis - part II: A case study in China. IEEE Trans. Power Syst. 28 (4), 3556–3565. http://dx.doi.org/10.1109/TPWRS.2013.2252028.

Marzebali, M.H., Mazidi, M., Mohiti, M., 2020. An adaptive droop-based control strategy for fuel cell-battery hybrid energy storage system to support primary frequency in stand-alone microgrids. J. Energy Storage 27, 101127. http://dx.doi.org/10.1016/j.est.2019.101127.

Mcgill, R., Torres-Olguin, R., Anaya-Lara, O., 2022. Generator response following as a primary frequency response control strategy for VSC-HVDC connected offshore windfarms.

Ming, H., Xia, B., Lee, K.Y., Adepoju, A., Shakkottai, S., Xie, L., 2020. Prediction and assessment of demand response potential with coupon incentives in highly renewable power systems. Protect. Control Modern Power Syst. 5 (1), 1–14.

Moorthi, V.R., Aggarwal, R.P., 1974. Damping effects of excitation control in load-frequency control system. Proc. Inst. Electr. Eng. 121 (11), 1409–1416.

Mudaheranwa, E., Sonder, H.B., Cipcigan, L., 2020. Feasibility study and impacts of EV penetration in Rwanda's MV distribution networks. In: 6th IEEE International Energy Conference, ENERGYCon , Sep. 2020. pp. 284–289. http://dx.doi.org/10.1109/ENERGYCON48941.2020.9236568.

Mudaheranwa, E., Sonder, H.B., Cipcigan, L., Ugalde-Loo, C.E., 2022. Estimation of Rwanda's power system inertia as input for long-term dynamic frequency response regulation planning. Electr. Power Syst. Res. 207, 107853.

Pappachen, A., Peer Fathima, A., 2021. Load frequency control in deregulated power system integrated with SMES-TCPS combination using ANFIS controller. Int. J. Electr. Power Energy Syst. 82, 519–534.

Parvania, S.M., 2014. ISO's optimal strategies for scheduling the hourly demand response in day-ahead markets. IEEE Trans. Power Appar. Syst. 29 (6), 2636–2645.

Prabha, Kundur, Balu, Neal J., Lauby, Mark G., 1994. Power system stability and control. vol. 7. McGraw-hill, New York.

Rahman, A., Saikia, L.C., Sinha, N., 2020. Load frequency control of a hydro-thermal system under deregulated environment using biogeography-based optimised three-degree-of-freedom integral-derivative controller. IET Gener. Transm. Distrib. 9, 2284–2293.

Ruiz, N., 2009. A direct load control model for virtual power plant management. IEEE Trans. Power Appar. Syst. 24 (2), 959–966.

Rwanda Utilities Regulatory Authority, 2022. Press release for electricity tariffs. [Online]. Available: https://rura.rw/fileadmin/publication/Press_release_for_Electricity_Tariffs.pdf, (Accessed 29 September 2022).

Saad, Y.E.M., Salama, M.M.A., Elshatshat, R.A., Ponnambalam, K., 2009. The operation of a distribution company under uncertainty: an overview. In: 2009 IEEE Power and Energy Society General Meeting PES ' 09. http://dx.doi.org/10.1109/PES.2009.5275857.

Saha, A., Saikia, L.C., 2018. Performance analysis of combination of ultra-capacitor and superconducting magnetic energy storage in a thermal-gas AGC system with utilization of whale optimization algorithm optimized cascade controller. J. Renew. Sustain. Energy 10, 014103. http://dx.doi.org/10.1063/1.5003958.

Sahin, E., 2020. Design of an optimized fractional high order differential feedback controller for load frequency control of a multi-area multi-source power system with nonlinearity. IEEE Access 8, 12327–12342. http://dx.doi.org/10.1109/ACCESS.2020.2966261.

Salama, H.S., Aly, M.M., Abdel, M., Vokony, I., 2019. Frequency and voltage control of microgrid with high WECS penetration during wind gusts using superconducting magnetic energy storage. Electr. Eng. 34, 234–244. http://dx.doi.org/10.1007/s00202-019-00821-w.

Sallam, A.A., Malik, O.P., analysis, Power.flow., 2015. Power system stability: modelling, analysis and control. pp. 107–130. http://dx.doi.org/10.1049/pbpo076e_ch5.

Sandels, C., Widén, J., Nordström, L., 2014. Forecasting household consumer electricity load profiles with a combined physical and behavioral approach. Appl. Energy 131, 267–278. http://dx.doi.org/10.1016/J.APENERGY.2014.06.048.

Saxena, P., Singh, N., Pandey, A.K., 2020. Enhancing the dynamic performance of microgrid using derivative controlled solar and energy storage based virtual inertia system. J. Energy Storage 31, 101613. http://dx.doi.org/10.1016/j.est.2020.101613.

Silva, S.S., Assis, T.M.L., 2020. Adaptive underfrequency load shedding in systems with renewable energy sources and storage capability. Electr. Power Syst. Res. 189, 106747. http://dx.doi.org/10.1016/j.epsr.2020.106747.

Singh, S.P., Prakash, T., Singh, V.P., 2020. Coordinated tuning of controller-parameters using symbiotic organisms search algorithm for frequency regulation of multi-area wind integrated power system. Eng. Sci. Technol. Int. J. 23 (1), 240–252.

Udoakah, Y.O., Mudaheranwa, E., Cipcigan, L., 2019. Dynamic modeling of energy consumption pattern of a typical nigerian average urban and rural household for microgrid pv design. In: Proceedings of 2019 IEEE PES Innovative Smart Grid Technologies Europe, ISGT-Europe 2019. http://dx.doi.org/10.1109/ISGTEUROPE.2019.8905464.

Ulbig, A., Borsche, T.S., Andersson, G., 2014. Impact of low rotational inertia on power system stability and operation. IFAC Proceedings Volumes (IFAC-PapersOnline) 19, 7290–7297. http://dx.doi.org/10.3182/20140824-6-za-1003.02615.

Veerasamy, V., Wahab, N.I.A., Ramachandran, R., Othman, M.L., Hizam, H., Kumar, J.S., Irudayaraj, A.X.R., 2022. Design of single-and multi-loop self-adaptive PID controller using heuristic based recurrent neural network for ALFC of hybrid power system. Expert Syst. Appl. 192, 116402.

Villena, J., Vigueras-Rodríguez, A., Gómez-Lázaro, E., FuentesMoreno, J.Á., Muñoz-Benavente, I., Molina-García, Á., 2015. An analysis of decentralized demand response as frequency control support under critical wind power oscillations. Energies 8 (11), 12881–12897. http://dx.doi.org/10.3390/en81112349.

Vinoth Kumar, N.J., Thameem Ansari, M.M., 2016. A new design of dual mode type-II fuzzy logic load frequency controller for interconnected power systems with parallel AC-DC tie-lines and capacitor energy storage unit. Int. J. Electr. Power Energy Syst. 82, 579–598. http://dx.doi.org/10.1016/j.ijepes.2016.03.063.

Wang, Y., Wan, C., Zhou, Z., Zhang, K., 2018. Improving deployment availability of energy storage with data-driven AGC signal models. IEEE Trans. Power Syst. 33, 4207–4217. http://dx.doi.org/10.1109/TPWRS.2017.2780223.

Wu, Y.K., Tang, K.T., 2019. Frequency support by demand response – Review and analysis. Energy Procedia 156, 327–331. http://dx.doi.org/10.1016/J.EGYPRO.2018.11.150.

Xi, L., Yu, L., Xu, Y., Wang, S., Chen, X., 2020a. A novel multi-agent DDQN-AD methodbased distributed strategy for automatic generation control of integrated energy systems. IEEE Trans. Sustain. Energy 11, 2417–2426. http://dx.doi.org/10.1109/TSTE.2019.2958361.

Xi, L., Yu, L., Xu, Y., Wang, S., Chen, X., 2020b. A novel multi-agent DDQN-AD methodbased distributed strategy for automatic generation control of integrated energy systems. IEEE Trans. Sustain. Energy. 11, 2417–2426. http://dx.doi.org/10.1109/TSTE.2019.2958361.

Xu, Y., Li, C., Wang, Z., Zhang, N., Peng, B., 2018. Load frequency control of a novel renewable energy integrated micro-grid containing pumped hydropower energy storage. IEEE Access 6, 29067–29077. http://dx.doi.org/10.1109/ACCESS.2018.2826015.

Xu, Y., Xie, L., Singh, C., 2011a. Optimal scheduling and operation of load aggregators with electric energy storage facing price and demand uncertainties. In: NAPS 2011-43rd North American Power Symposium. http://dx.doi.org/10.1109/NAPS.2011.6024888.

Xu, Y., Xie, L., Singh, C., 2011b. Optimal scheduling and operation of load aggregators with electric energy storage facing price and demand uncertainties. http://dx.doi.org/10.1109/NAPS.2011.6024888.

Zhu, Q., Jiang, L., Yao, W., Zhang, C.-K., Luo, C., 2017a. Robust Load Frequency Control with Dynamic Demand Response for Deregulated Power Systems Considering Communication Delays.

Zhu, Q., Jiang, L., Yao, W., Zhang, C., Luo, C., 2017b. Robust load frequency control with dynamic demand response for deregulated power systems considering communication delays. Electrical Power Components Syst. 45, 75–87. http://dx.doi.org/10.1080/15325008.2016.1233300.